1971

Propagation of cylindrical magnetic domains

Yeou-ren Lai
Iowa State University

Propagation of cylindrical magnetic domains

by

Yeou-ren Lai

A Dissertation Submitted to the

Graduate Faculty in Partial Fulfillment of

The Requirements for the Degree of

DOCTOR OF PHILOSOPHY

Major Subject: Electrical Engineering

Approved:

Signature was redacted for privacy.

In Charge of Major Work

Signature was redacted for privacy.

For the Major Department

Signature was redacted for privacy.

For the Graduate College

Iowa State University
Ames, Iowa

1971

TABLE OF CONTENTS

I. INTRODUCTION

The use of magnetic storage techniques in digital memory applications has been extremely successful. Magnetic memory elements are generally simple nonvolatile electrically passive structures permitting highly reliable operation at low cost, low power, and high speed. For some time, the possibility of using the controlled motion and interactions of magnetic domain boundaries to propagate, store, and process digital information has been envisioned. Lossless transfer of information is obtained by the simple displacement of the domain boundaries; fan-out or gain is easily produced by the expansion of an existing domain. Various techniques and materials allow binary information to be stored as the presence or absence of domains of reversed magnetization with an initially saturated magnetic background, permitting these information-bearing domains to be controllably stepped along some collection of paths under the action of a time-varying magnetic field. Streams of information propagate along these paths with means provided for introducing and removing domains and for sensing the stored domains as they propagate past input and output locations. Some of these techniques permit logic and gating functions to be performed within the memory medium either through the mutual interaction of domains or domain walls or by their interaction with an applied magnetic field.

It has been possible to produce the action described above by using thin magnetic films (1-4) and single crystal platelets exhibiting a uniaxial magnetic anisotropy (5, 6). In the case of thin magnetic films, a uniaxial anisotropy is produced in the plane of the film. Magnetization

also lies in the plane of the film and a magnetic domain is seen to be an isolated reverse magnetization area bounded by a domain wall. Due to anisotropy inherent in the film itself, the disparity in the propagation modes for the easy and hard directions exists (4). Complete generality in the propagation and interactions of magnetic domains, however, demands that the magnetization be aligned to lie normal to the surface of the film. Furthermore, it would be useful if the magnetic properties were isotropic in the plane of the film. Cylindrical magnetic domains exhibited in the single crystal platelets, such as orthoferrites, meets these conditions.

The approach using cylindrical magnetic domains in device applications has currently received considerable attention. The properties of the materials used require the magnetization to lie normal to the surface of the plate. The modes of operation of devices constructed from such materials are classified according to the effect of wall motion coercivity (7). In the case of very high wall motion coercivity, the application of applied field determines the initial domain configuration which is then maintained by coercivity. For very low wall coercivity, on the other hand, the saturation magnetization, wall energy, plate thickness, and bias field determine the domain size and shape. Between these two extremes, there is a continuum of intermediate modes. The work in this thesis will concern only the low coercivity mode and specifically, right circular cylindrical domains in the plates of uniform thickness. When observed by means of the Faraday effect, cylindrical domains have the

appearance of bubbles and therefore are colloquially referred to as "bubbles".

A theory of cylindrical magnetic domains has been formulated by Thiele (7, 8) and investigated experimentally by Bobeck and the others (5, 6, 9). The static analysis has been presented in detail (5, 7, 8), but the dynamic analysis has not yet been given explicitly in the literature. The dynamic theory is plagued by such intractable constructs as integrals of elliptic integrals. Consequently, recourse to graphical methods or numerical procedures is required to provide the general picture of domain dynamics. In analysis of both statics and dynamics, it is commonly assumed that domain walls are cylindrical, have zero width, and have a definite energy per unit area which is independent of wall orientation or curvature, and that the magnetization lies perpendicular to the surface of the plate. The validity of these assumptions has been discussed by Thiele (7). Consequently, the domain structure model used in this thesis will be within the range of this validity of these assumptions.

Domains in materials with required properties are maintained in the preferred cylindrical form by an overall uniform bias field applied normal to the platelet surface. This bias field is directed antiparallel to the magnetization of the domain and has a magnitude which is within the stability range. An increase in the bias field decreases the domain diameter and vice versa. Now if the bias field is nonuniform and not symmetrical with respect to the center of the domain, the domain will experience a net unbalanced force due to different values of bias field

at each point of the wall. This unbalance force combined with the stiffness of the domain wall causes the domain to move as entity in the direction of the net force. For example, if the bias field is a linear function of x only, the domain will move in the direction of decreasing bias field magnitude provided that the driving force is greater than the domain coercivity. As the domain moves, the magnitude of the average bias field effective on the domain decreases and if the domain is allowed to travel a sufficient distance, it will reach a point where it will run into a strip domain. Cylindrical magnetic domain can be manipulated, therefore, by producing local field gradients that do not allow the domains to run out of the stable bias field range.

When a uniform field gradient is applied, the domain will experience a force attempting to move it toward a position of reduced bias. The propagating velocity of the domain will be constant provided $\Delta H > (8/\pi)H_c$, where H_c is the wall coercivity and ΔH is the maximum difference in the applied field across the domain diameter. In practice the applied local field to a cylindrical domain, however, is not simply a uniform gradient. In this case the response will be complex and could involve a change in domain size and shape, motion at a nonuniform rate, or even the collapse of a domain. Experimentally, it has been observed (10) that the shape of domains changes as they propagate and the domain motion is highly nonuniform with velocity varying widely with position along the propagating channel. Since demand for high data rates is essential in device applications, the study of domain dynamics under nonuniform field gradient allows one to see how domain propagation fails at higher frequencies in

a given structure under dynamic conditions and thus will be a useful aid in the design of propagating structures.

To study the domain dynamics, the effect of the additional nonuniformities is taken into account by Fourier decomposition of the z-average z component of the applied field at the domain with respect to angle, where the z direction is normal to the plane of the platelet. The additional energy term arising from this nonuniform field is added to the total domain energy and then the total energy variation is calculated. Since "wall mass" is negligibly small in practical cases, the kinetic energy term is ignored and only the dissipation is considered. The method used to take dissipative effects into account is to compute the power dissipation produced by a general variation in domain shape using the wall dissipation equation and then to set this equal to the power produced by the variation. When this is done, the constant term of the applied field determines domain size, the θ term translates the domain, and the $n\theta$ terms, for $n \geq 2$, deform the domain. The results show that the domain propagates at nonuniform rate and the magnitude of domain velocity depends on the variation of the applied field except for the case of uniform field gradient. Assuming uniform coercivity and neglecting the coupling terms, formulae for change in domain size and shape have been established.

In order to utilize cylindrical domains in shift registers, memories, and logic circuits, motion of domains in discrete steps is required at specific times. Therefore, highly localized fields are needed. Such fields can be produced by current-carrying conductor circuit or all

permalloy propagating circuit. In the first case, thin film techniques are used to fabricate the conductive loops placed flat on a platelet surface. The circuit is operated with a biphase propagating source. An array of permalloy dots are used to introduce an asymmetry into the conductor pattern so that directionality is achieved. These asymmetry permalloy dots, which provide low energy sites for the domains, places domains in a consistent preferred position prior to each propagating phase. In the case of all permalloy propagating circuit, the permalloy is used to interact with, and thereby propagate domains in the platelet. There are two such general classes of circuits. The first class, devised the angelfish circuit, utilizes the fact that a cylindrical domain can be modulated in size by increasing or decreasing the bias field. Motion is achieved by maneuvering this pulsating cylindrical domain in and out of asymmetrical energy traps. In the second method of permalloy circuit propagation an in-plane rotating field acting on a structured permalloy pattern generates traveling positive and negative magnetic poles to selectively attract and repel and thereby control the domain motion. A variety of permalloy patterns are suitable and commonly used are T-bar and Y-bar.

Of these various methods of domain propagation, T-bar or Y-bar propagation seems to be suitable for practical applications. The reasons lie in the elimination of the need for a fabrication of small current-carrying conductors, the relative ease in generating drive fields at low power levels, and the logic capabilities inherent in this mode of propagation. Consequently, the dynamic phenomena of this type of domain propaga-

tion are investigated in this thesis. The magnetic fields produced by magnetized permalloy bars induced by the applied transverse uniform rotating field are calculated. With such fields domain translation and change in domain size and shape are investigated using previously calculated equations. The calculation shows that the velocity of domain translation is highly nonuniform due to highly nonuniform field gradient. Domain size and shape also change when the domain is in motion. Variation of the width of permalloy bars shows that the narrower one has higher initial driving field and more uniform speed.

Finally, in this thesis the force exerted by a permalloy bar on a magnetic domain is discussed. Without applying the tranverse rotating field, there exists a magnetostatic interaction between bubble domains and permalloy films. Since the permalloy films serve as localized flux closure paths thereby reducing the magnetostatic energy, the cylindrical domain prefers a position in contact with the permalloy. Consequently, there exists a force exerted by permalloy films on a cylindrical domain. In order to evaluate the force, the permalloy film is assumed to be thin enough so that the magnetization induced in the permalloy by the bubble field is in the plane of the film. The radial bubble field is determined by integrating the magnetic field from a circular current loop over the bubble thickness and then changing the source by the standard method. The resulting field is a function of the complete elliptic integrals of the first and second kind. Magnetization induced in the permalloy is approximated by idealized and linearized model of M-H curve. The result of numerical calculation of the force is given in this thesis. It shows

that there exists an attractive force on the bubble when the bubble is approaching to the permalloy and that the force reaches maximum just after the leading edge of the domain is at the position in contact with the permalloy. In the reverse, to pull the bubble completely off the permalloy film a large amount of external force is needed to counter-balance this force. Consequently, the force due to the magnetostatic interaction also affects the propagation of cylindrical domains in permalloy circuit. Extra power input is needed especially at which the bubble is about completely off the permalloy. Calculation of the force used here is also useful in designing the wedge-shaped films in the "angelfish" circuit. The radial bubble field can be used in designing domain detector using magnetoresistive detection.

II. LITERATURE REVIEW

Magnetic domain behavior in single-crystal magnetic oxides has been studied extensively over the last several decades. These investigations, both theoretical and experimental, are an attempt to better understand these materials and their complex domain structures. Recently, magnetic domains in single-crystal oxides have been utilized in memory logic devices. Extensive studies of cylindrical magnetic domains have been accomplished by the Bell Telephone Laboratories group and the others. Cylindrical magnetic domains are required to have the following properties (5, 11): (1) the domains exist in a plate of magnetic materials of uniform thickness, (2) the magnetization in the plate lies normal to the surface of the plate by uniaxial anisotropy, (3) domain-wall width is small compared to domain diameter, (4) wall-motion coercivity is sufficiently small so that domain size and shape are independent of coercivity. The material requirements are also determined from a combination of such engineering requirements as cost, room temperature operation, the availability of materials, and the restrictions arising from the static stability and mobility condition (7, 8).

A general requirement for the existence of cylindrical domains with magnetization perpendicular to a thin plate of material is $H_k/4\pi M_s > 1$ (8, 12), where H_k is the uniaxial anisotropy field and M_s is the saturation magnetization. Cylindrical domains are only observable when the plate thickness and domain diameter are some small multiple of the characteristic length, $\ell = \sigma_w/4\pi M_s^2$ (7, 8), where σ_w is the wall energy density. The

ratio of domain-wall width to this characteristic length is $(\pi/2)(4\pi M_s/H_k)$ (13). Consequently, the assumptions that the magnetization lies only along the plate normal, domains do not spontaneously nucleate, and the wall has negligible width improve as $H_k/4\pi M_s$ is increased. However, from the point of view of device design it is not desirable for the anisotropy field to be much greater than $4\pi M_s$. The reason for this is provided by general mobility relation. Under the assumption of Gilbert damping, the wall mobility can be expressed as $\mu_w = 4|\gamma|A/\alpha\sigma_w$ (14), where A is the exchange constant, α is the Gilbert damping constant, and $|\gamma|$ is the gyromagnetic ratio. Since the wall width is defined by $\ell_w = 4\pi A/\sigma_w$ (13), the wall mobility may be written in the form, $\mu_w = |\gamma|\ell_w/\alpha\pi$. It can be seen that for a given amount of damping, the wall velocity will be proportional to the wall width. Therefore, the preferred value of H_k when high domain mobility is desired is some small multiple of $4\pi M_s$.

There are a number of different classes of magnetic materials that will support isolated circular domains covering a several-orders-of-magnitude range of diameters. The desired domain diameter, commensurate with present technological ability to construct control structures, is in the 1 μm-to-10 μm range. Ideal circular domain device materials are homogeneous and have the desired properties intrinsically. Published articles on bubble domain materials have described work with single crystals of orthoferrites (5, 6, 15), hexagonal ferrites (16), and magnetic garnets (17-21). The main parameters involved in determining bubble diameter, d, are the magnetic exchange energy, E_{ex}, the uniaxial

magnetocrystalline anisotropy, K_u, and the magnetization, M_s, of the crystal and generally can be expressed as $d \propto E_{ex}^{\frac{1}{2}} K_u^{\frac{1}{2}} M_s^{-2}$. The orthoferrites meet most of the requirements for bubble domain devices. Their principal deficiency is a high K_u/M_s ratio. As a result the diameter is generally larger than desirable. Suitable K_u/M_s ratios are realizable in the hexagonal ferrites; however, bubble domain mobility is disappointingly slow (22). The magnetically uniaxial garnets are in some respects a compromise. The mobility values are intermediate to those of the hexagonal ferrites and the othoferrites (22, 23).

Two important features toward device applications of the cylindrical domains are the behavior of domain size under variations in temperature and domain-wall mobility. If a bubble domain device is to operate in an enviroment that permits temperature excursions, the influence of those changes on the domain diameter must be established to determine the temperature limit for reliable performance. Moreover, for fixed values of bubble diameter and applied field gradient, the maximum data rate attainable in bubble devices is determined by the domain mobility (22). The temperature dependence of the domain diameter has been studied in a number of rare-earth orthoferrites by Rossol (24). All the materials measured show that the domain diameter increases with decreasing the temperature. The Sm-Tb mixture, which has the smallest cylindrical domains, has the largest fractional change in diameter with temperature. The least temperature sensitive of the materials is $YFeO_3$. Heinz et al. (23) have measured the temperature dependence of the domain diameter in a Gd:YIG film. It shows that the domain diameter of this garnet is

significantly less influenced by temperature change than is that of orthoferrites. Wall mobilities in bubble materials have been measured by modulation of the equilibrium position of the domain wall (25), by transient bubble collapse technique (22), by observation of the response of a domain wall in the strip domain configuration to an impulse field (26), by investigation of the translational dynamics of a domain moving around the circumference of a permalloy disk (27), and by direct measurement of the velocity of a domain in a known field gradient (23, 28). Room temperature values of mobility for several orthoferrites fall in the range from 100-1000 cm/sec-Oe (25). Therefore, the temperature dependence of the mobility has substantial differences among them. Domain-wall mobility in $YFeO_3$ has been observed to have values from 6000 cm/sec-Oe at $300^{o}K$ to 50000 cm/sec-Oe at $77^{o}K$ (29). Wall mobility in magnetically uniaxial garnets has the value a little smaller than orthoferrites (22, 23).

III. ANALYSIS AND APPLICATION OF PROPAGATION OF CYLINDRICAL MAGNETIC DOMAINS

A. The Static Theory of Magnetic Bubble Domains

The static theory of cylindrical magnetic domains which provides conditions governing the size and stability of circular cylindrical domains in the plates of uniaxial magnetic materials was developed by Thiele (7, 8). Figure 1 shows the model for the domain structure from which the theory was developed. The model represents a single isolated domain in a plate of magnetic material of uniform thickness, h, and an infinite extent of the plane, $r_f = \infty$. Everywhere within the material the magnetization has a uniform saturation magnitude, M_s, directed along the downward plate normal (-z direction) within the domain and along the upward plate normal elsewhere within the material. The domain wall is assumed to be independent of z and to have a width which is negligible in comparison to the domain radius. It is assumed that the domain wall energy density, σ_w, is taken to be independent of both orientation and curvature. The spatially uniform applied bias field, H, is taken positive when directed upward, the direction tending to collapse the domain. In order for the domains of the types to be considered here to exist, the material is required to have that

$$K_u > 2\pi M_s^2 \tag{1a}$$

or

$$H_k > 4\pi M_s \tag{1b}$$

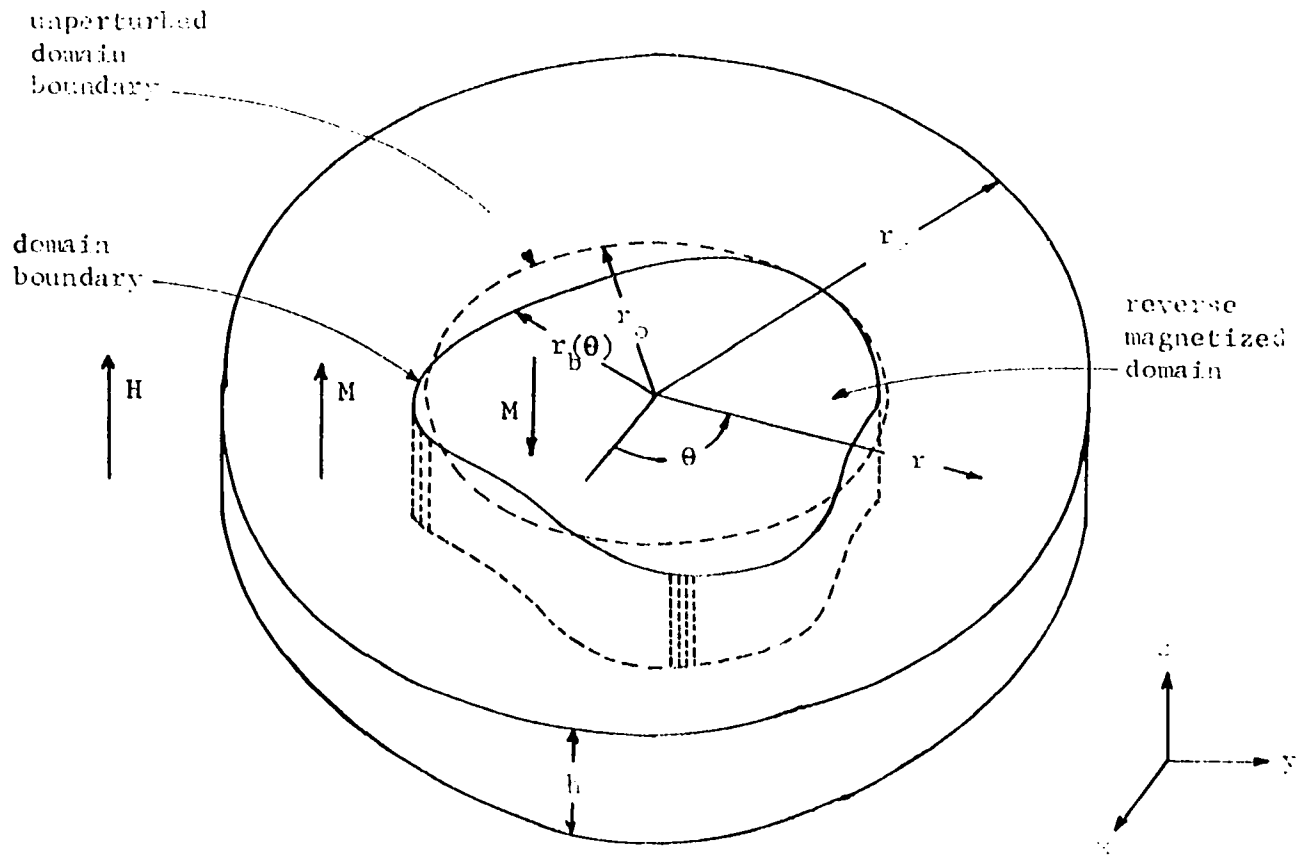

Figure 1. Domain configuration and coordinate system

where K_u is the uniaxial anisotropy constant and H_k ($=2K_u/M_s$) is the uniaxial anisotropy field.

The domain radius function, $r_b(\theta)$, which is expanded in the series

$$r_b(\theta) = r_o + \Delta r_o + \sum_{n=1}^{\infty} \Delta r_n \cos [n(\theta - \theta_n - \Delta\theta_n)] \tag{2}$$

describes the domain size and shape. The Δr_n and $\Delta\theta_n$ describe small variations in domain size and shape from a circular domain of radius $r_b(\theta) = r_o$. Since only near circular domains are of interest here, the condition

$$|r_o| \gg |\Delta r_o| + \sum_{n=1}^{\infty} n|\Delta r_n| \tag{3}$$

is imposed to assure that the radius is single-valued and smooth.

The total domain energy,

$$E_T = E_W + E_H + E_M \tag{4}$$

is the sum of three terms. The wall energy, E_W, is the product of the wall energy density and the wall area. The applied field interaction energy, E_H, is proportional to the product of the domain volume and the external field interaction energy. The last term, E_M, is the internal magnetostatic energy of the domain. The variation in the total energy when the Δr_n and $\Delta\theta_n$ are varied is

$$\Delta E_T = \sum_{n=0}^{\infty} \left[\left(\frac{\partial E_T}{\partial r_n}\right)_o \Delta r_n + \left(\frac{\partial E_T}{\partial \theta_n}\right)_o \Delta \theta_n \right]$$

$$+ \frac{1}{2} \sum_{n=0}^{\infty} \sum_{m=0}^{\infty} \left[\left(\frac{\partial^2 E_T}{\partial r_n \partial r_m}\right)_o \Delta r_n \Delta r_m + 2\left(\frac{\partial^2 E_T}{\partial r_n \partial \theta_m}\right)_o \Delta r_n \Delta \theta_m \right.$$

$$\left. + \left(\frac{\partial^2 E_T}{\partial \theta_n \partial \theta_m}\right)_o \Delta \theta_n \Delta \theta_m \right] + 0_3 \qquad (5)$$

where in the energy derivatives the independent variables, Δr_n and $\Delta \theta_n$, have been abbreviated as r_n and θ_n for compactness, the subscript o refers to evaluation of the partial derivatives at the circular domain state, $r_b(\theta) = r_o$, and 0_3 refers to terms of order three and higher. The first partial derivatives of the energy, $(\partial E_T/\partial r_n)_o$ and $(\partial E_T/\partial \theta_n)_o$, are the generalized forces of the system, while the second derivatives of the energy determine the stability conditions.

The derivatives of the total energy with respect to Δr_n and $\Delta \theta_n$ are obtained by differentiating the integrals which form the terms of Equation 4 and evaluating the resulting integrals for the case of a strictly circular domain. The result of the total energy variation expression, Equation 5, is (7)

$$\Delta E_T = \left[2\pi h \sigma_w + 4\pi r_o h M_s H - (2\pi h^2)(4\pi M_s^2) F\left(\frac{2r_o}{h}\right) \right] \Delta r_o$$

$$+ \frac{1}{2} \left[4\pi h M_s H - (4\pi h)(4\pi M_s^2) \frac{\partial F\left(\frac{2r_o}{h}\right)}{\partial \left(\frac{2r_o}{h}\right)} \right] (\Delta r_o)^2$$

$$+\frac{1}{2}\sum_{n=1}^{\infty}\{\frac{\pi}{r_o}h\sigma_w n^2 + 2\pi hM_s H - (2\pi h)(4\pi M_s^2)\frac{\partial F(\frac{2r_o}{h})}{\partial(\frac{2r_o}{h})}$$

$$+ h(4\pi M_s^2)\frac{2r_o}{h}[L_n((\frac{h}{2r_o})^2) - L_n(0)]\}(\Delta r_n)^2 + 0_3 \qquad (6)$$

where $F(x)$ and $L_n(x)$ are functions of complete elliptic integrals of the first and second kind. Since the stability of the domains is only of interest here when the equilibrium condition is satisfied, the force equation may be used to eliminate the applied field from the second variations. To write the energy variation expression in a normalized form, energy is measured in units of $4(2\pi M_s^2)(\pi h^3)$, the applied field is measured in units of the magnetization, $H/4\pi M_s$, and the wall energy is written in terms of the characteristic length of the material

$$\ell = \frac{\sigma_w}{4\pi M_s^2} \qquad (7)$$

The resulting normalized form of energy expression is

$$\frac{\Delta E_T}{4(2\pi M_s^2)(\pi h^3)} = [\frac{\ell}{h} + \frac{d}{h}\frac{H}{4\pi M_s} - F(\frac{d}{h})]\frac{\Delta r_o}{h}$$

$$+\frac{1}{2}\{-(\frac{2h}{d})[\frac{\ell}{h} - S_o(\frac{d}{h})](\frac{\Delta r_o}{h})^2$$

$$+\sum_{n=2}^{\infty}(n^2-1)(\frac{h}{d})[\frac{\ell}{h} - S_n(\frac{d}{h})](\frac{\Delta r_n}{h})^2\} + 0_3 \qquad (8)$$

where d is the domain diameter, $2r_o$, $S_o(x)$ is a function of $F(x)$, and $S_n(x)$ is a function of $L_n(x)$. $F(d/h)$ and $S_n(x)$ are defined as the force and stability functions, respectively. The force function and stability functions from n=0 to n=10 are plotted in Figure 2.

The domain is in equilibrium when all of the first order variations of the total energy with respect to the Δr_n and $\Delta\theta_n$ are zero. By inspection of Equation 8, it can be seen that the domain is in equilibrium when it is a circular cylinder having a diameter which is a solution to the normalized force equation,

$$\frac{\ell}{h} + \frac{d}{h}\frac{H}{4\pi M_s} - F\left(\frac{d}{h}\right) = 0 \qquad (9)$$

Solutions to the equilibrium problem may be discussed either in terms of the equivalent fields as was done by Bobeck (5) or in terms of Equation 9 with graphical method done by Thiele (7). By either methods, it shows that a stable cylindrical domain can be obtained by choosing proper thickness, h, and the applied bias field, H. Figure 3 shows an example of cylindrical domain size as a function of an applied field.

The sign of the second variation of the total domain energy produced by a weak variation in shape characterizes the stability of a cylindrical domain. In the equilibrium energy expression, Equation 8, the only nonzero quadratic coefficients are the coefficients of the $(\Delta r_n)^2$, $n \neq 1$. As required by the cylindrical symmetry of the system, the domain is completely metastable with respect to angle. Consequently, from Equation 8 it can be seen that the domain is stable with respect to an arbitrary variation in shape when

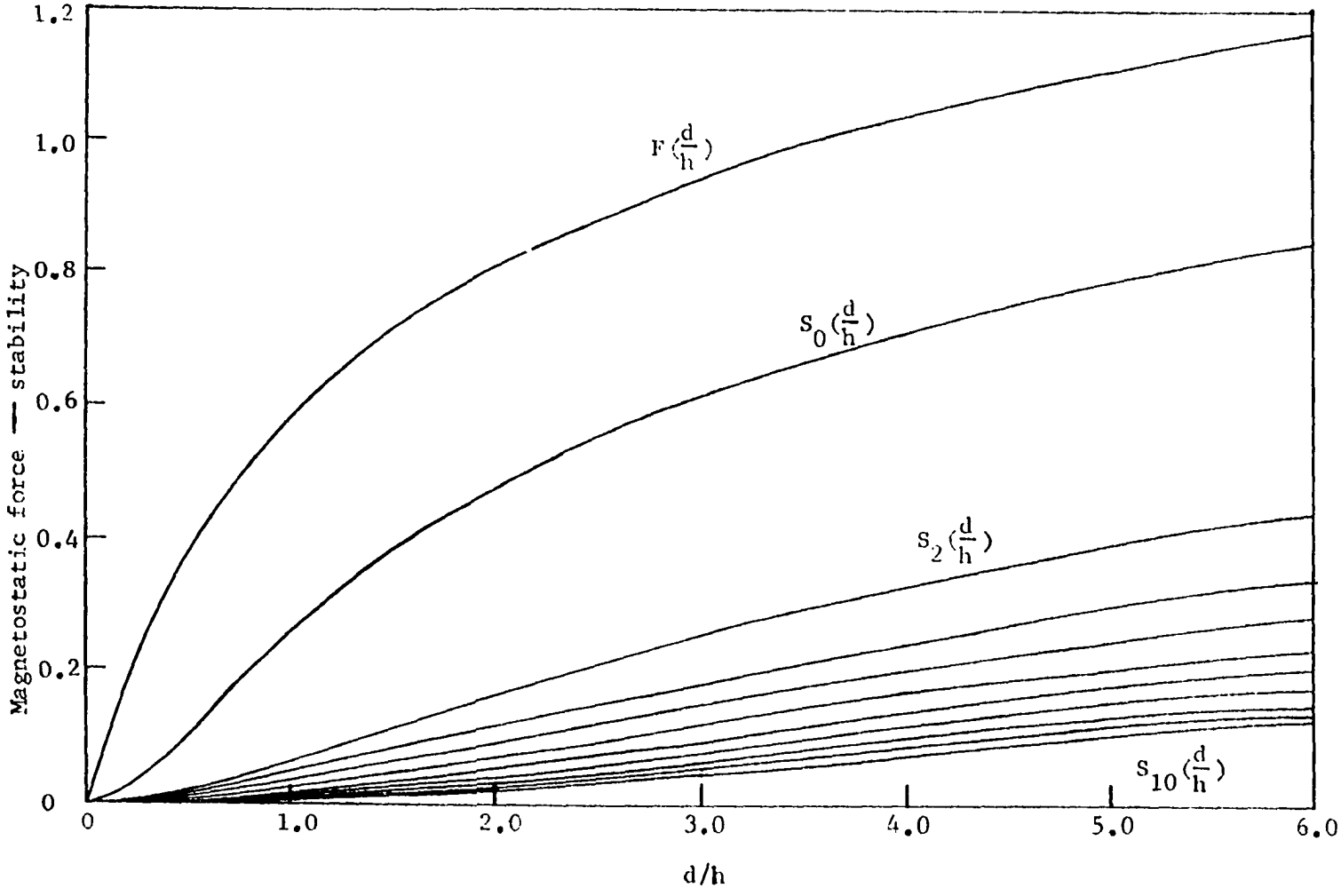

Figure 2. The magnetostatic radial force function and stability functions

Figure 3. Cylindrical domain size as a function of an applied bias field

Figure 4. Cylindrical domain diameter as a function of platelet thickness

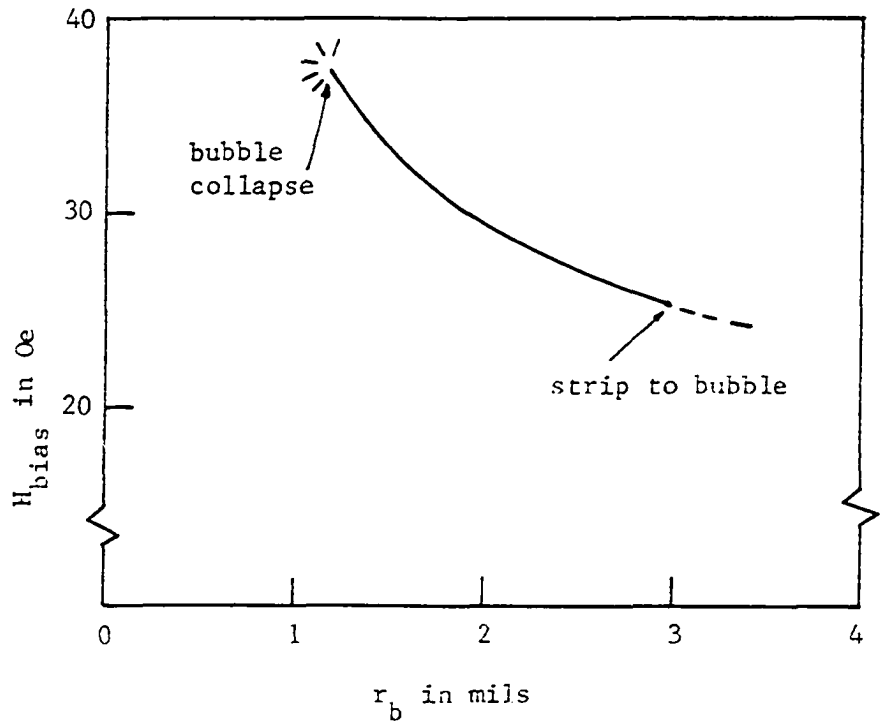
40
30
20
bubble
collapse
strip to bubble
H_{bias} in Oe
0
1
2
3
4
r_b in mils

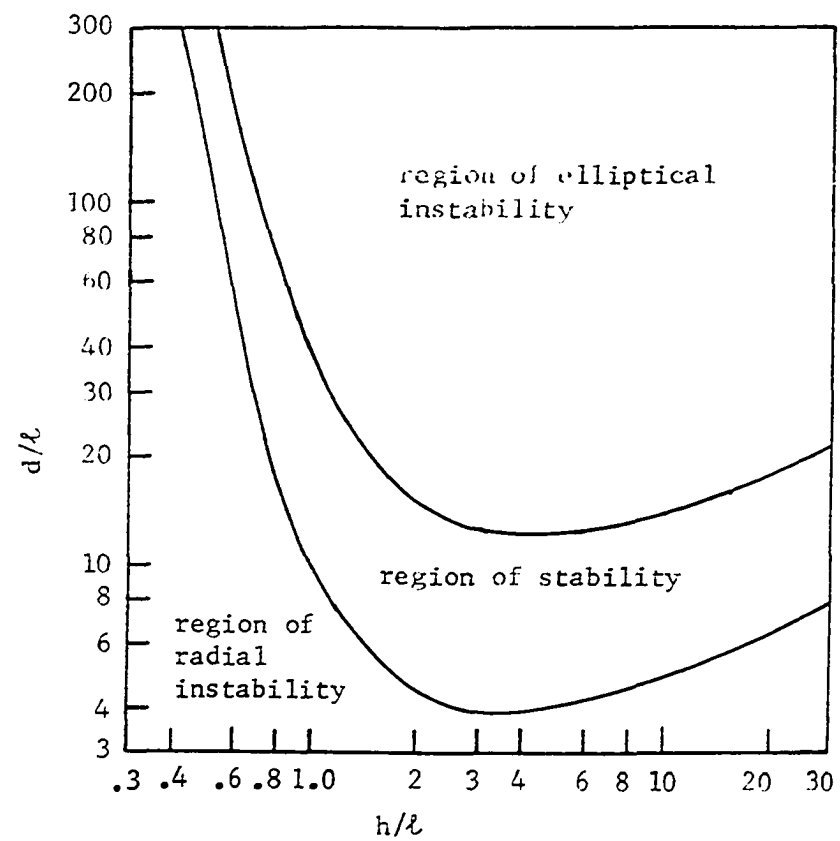
300
200
100
80
60
40
30
20
10
8
6
4
3
region of elliptical instability
region of stability
region of radial instability
d/ℓ
.3 .4 .6 .8 1.0 2 3 4 6 8 10 20 30
h/ℓ

$$\left[\frac{\ell}{h} - S_o\left(\frac{d}{h}\right) \right] < 0 \tag{10a}$$

and

$$\left[\frac{\ell}{h} - S_n\left(\frac{d}{h}\right) \right] > 0 , \quad n \geq 2 \tag{10b}$$

or

$$S_o\left(\frac{d}{h}\right) > \frac{\ell}{h} > S_n\left(\frac{d}{h}\right) \tag{10c}$$

Since the stability functions have the property (Figure 2),

$$S_{n+1}\left(\frac{d}{h}\right) < S_n\left(\frac{d}{h}\right) \tag{11}$$

the condition for total stability reduces to

$$S_o\left(\frac{d}{h}\right) > \frac{\ell}{h} > S_2\left(\frac{d}{h}\right) \tag{12}$$

This determines the upper and lower limits on cylindrical domain diameters which are boundaries of the region of possible device operation. Figure 4 is a plot of these diameters measured in units of the characteristic length, ℓ, as function of the thickness measured in units of ℓ. The smallest stable domain attainable is about $d/h=1.2$ and $\ell/h=0.3$, or

$$d_{min} \simeq 4\ \ell \tag{13}$$

More thorough discussions of stability considerations were given by Thiele (8, 30).

B. Dynamics of Magnetic Bubble Domains Under Nonuniform Applied Field

1. General energy variation expression

The static theory of magnetic bubble domains provides the equilibrium and stability conditions of circular cylindrical domains. The generalized force, Equation 9, determines the size of the bubble domains and Equation 12 provides the stable range of the bubble domains. Cylindrical domains may, however, be propagated by gradients in any of the independent parameters which determine the total domain energy (31). These parameters are the applied field, H, the plate thickness, h, the saturation magnetization, M_s, and the wall energy density, σ_w. The domain radius, r_o, is not an independent parameter for domains in equilibrium but is determined once the other parameters are specified. In most device applications, cylindrical domains are most easily propagated by gradients in the applied field (6, 9). Consequently, the following analysis of the domain dynamics will be devoted to the case that the bubble domains are propagated by gradients in the applied field.

The bubble domains are maintained in the preferred cylindrical form by an overall uniform bias field applied normal to the platelet surface. As shown in Figure 3, an increase in the bias field decreases the domain diameter and vice versa. Now consider the reaction of a cylindrical domain subjected to a nonuniform rather than uniform field. The response will be complex and could involve changes in size and shape, motion at a nonuniform rate, or even the collapse of a domain. Consequently, except the case in which a uniform field gradient is applied, it is convenient

to treat the dynamic problem locally. The domain configuration at any instant will be the same as shown in Figure 1, except the applied field. Under the same assumptions as in the static case, only the component of the applied field normal to the platelet surface will interact with the domain. Suppose in addition to the uniform bias field that a nonuniform z-average z-component field is applied and has the form of

$$\vec{H}_a = - \vec{i}_z (H_o + H_1 r \cos\theta + H_2 r^2 \cos 2\theta) \tag{14}$$

where θ is the angle measured from the +x direction and $\vec{i}_z$ is the unit vector along the +z direction. It can be seen that H_o is the average field at the center of the domain and H_1 and H_2 account for the linear and quadratic field gradients, respectively. More general form of the applied field can be obtained by an infinite Fourier series expansion. Here only terms up to the second order will be considered. The coordinate system of this field is considered to follow the domain movement with the origin at the center of the domain so that the magnitude of H_a changes during the domain propagation.

When the nonuniform field is applied, only the applied field interaction energy term, E_H, will be different from the static case in the total energy Equation 4. The same radius Equation 2 will be used in the calculation of E_H in the dynamic case. The magnetization of the platelet may be written as

$$\vec{M} = \vec{i}_z M_s \{1 - 2u[r_b(\theta) - r]\}\ u(z + \tfrac{h}{2})\, u(-z + \tfrac{h}{2}) \tag{15}$$

where u(x) is the unit step function,

$$u(x) = \begin{cases} 0 , & x < 0 \\ \frac{1}{2} , & x = 0 \\ 1 , & x > 0 \end{cases} \tag{16}$$

The interaction energy of the magnetization with the externally applied field is then

$$E_H = -\int_V \vec{M} \cdot \vec{H}_a \, dV = -\int_{-\infty}^{\infty} \int_0^{2\pi} \int_0^{\infty} M_s H_a r \, dr \, d\theta \, dz \tag{17}$$

Substituting the expression for the applied field, Equation 14, and the magnetization configuration, Equation 15, into the applied field interaction energy expression, Equation 17, yields

$$E_H = M_s \int_0^{2\pi} \int_0^{\infty} \int_{-\infty}^{\infty} \{1 - 2u[r_b(\theta) - r]\} u(z + \tfrac{h}{2}) \, u(-z + \tfrac{h}{2})$$
$$(H_o + H_1 r \cos\theta + H_2 r^2 \cos 2\theta) \, r \, dr \, d\theta \, dz \tag{18}$$

Changing the order of integration and then integrating, it becomes

$$E_H = -M_s h H_o \int_0^{2\pi} r_b^2(\theta) d\theta - \frac{2}{3} M_s h H_1 \int_0^{2\pi} r_b^3(\theta) \cos\theta \, d\theta$$
$$- \frac{1}{2} M_s h H_2 \int_0^{2\pi} r_b^4(\theta) \cos 2\theta \, d\theta + \text{constant} \tag{19}$$

$$= -(E_H^0 + E_H^1 + E_H^2) + \text{constant} \tag{20}$$

where

$$E_H^0 = M_s h H_o \int_0^{2\pi} r_b^2(\theta) d\theta \tag{21}$$

$$E_H^1 = \frac{2}{3} M_s h H_1 \int_0^{2\pi} r_b^3(\theta) \cos\theta \, d\theta \tag{22}$$

$$E_H^2 = \frac{1}{2} M_s h H_2 \int_0^{2\pi} r_b^4(\theta) \cos 2\theta \, d\theta \tag{23}$$

The infinite constant is independent of the Δr_n and $\Delta\theta_n$ and does not contribute to the derivatives of the energy.

The derivatives of the applied field interaction energy are computed by substituting the wall shape expression, Equation 2, into the energy expression, Equation 19, or Equations 21-23. Evaluation of the first and second partial derivatives of the energy for $r_b(\theta) = r_o$ (see Appendix A) yields

$$\left(\frac{\partial E_H^0}{\partial r_o}\right)_o = 4\pi r_o h M_s H_o \tag{24a}$$

$$\left(\frac{\partial^2 E_H^0}{\partial r_o^2}\right)_o = 4\pi h M_s H_o \tag{24b}$$

$$\left(\frac{\partial^2 E_H^0}{\partial r_n^2}\right)_o = 2\pi h M_s H_o \quad , \qquad n \geq 1 \tag{24c}$$

$$\left(\frac{\partial E_H^1}{\partial r_1}\right)_o = 2\pi r_o^2 h M_s H_1 \cos\theta_1 \tag{25a}$$

$$\left(\frac{\partial^2 E_H^1}{\partial r_n \partial r_m}\right)_o = \begin{cases} 4\pi r_o h M_s H_1 \cos\theta_1 (\delta_{n1}\delta_{m0} + \delta_{n0}\delta_{m1}) \\ \\ 2\pi r_o h M_s H_1 \delta_{n,m\pm1} \cos(n\theta_n - m\theta_m) \quad , \quad n,m \geq 1 \end{cases} \tag{25b}$$

$$\left(\frac{\partial^2 E_H^1}{\partial r_n \partial \theta_m}\right)_o = -2\pi r_o^2 h M_s H_1 \delta_{m1}\delta_{n1} \sin\theta_1 \tag{25c}$$

$$\left(\frac{\partial E_H^2}{\partial r_2}\right)_o = 2\pi r_o^3 h M_s H_2 \cos 2\theta_2 \tag{26a}$$

$$\left(\frac{\partial^2 E_H^2}{\partial r_n \partial r_m}\right)_o = \begin{cases} 6\pi r_o^2 h M_s H_2 (\delta_{m0}\delta_{n2} + \delta_{n0}\delta_{m2}) \cos 2\theta_2 \\ 3\pi r_o^2 h M_s H_2 [\delta_{m1}\delta_{n1} \cos 2\theta_1 + \delta_{n,m\pm 2} \cos(n\theta_n - m\theta_m)], \\ \qquad\qquad n,m \geq 1 \end{cases} \tag{26b}$$

$$\left(\frac{\partial^2 E_H^2}{\partial r_n \partial \theta_m}\right)_o = -2\pi r_o^3 h M_s H_2 \delta_{m2}\delta_{n2} \sin 2\theta_2 \tag{26c}$$

where δ_{mn} is the Kronecker delta function. All the other first and second derivatives of the applied field interaction energy are zero.

Now adding these derivatives into the total energy variation expression for the static case, Equation 6, yields the general energy variation under the nonuniform applied field which can be summarized as

$$\begin{aligned} \Delta E_T = {} & \left[2\pi h\sigma_w + 4\pi r_o h M_s (H - H_o) - (2\pi h^2)(4\pi M_s^2) F\left(\frac{2r_o}{h}\right)\right](\Delta r_o) \\ & + \frac{1}{2}\left[4\pi h M_s (H - H_o) - (4\pi h)(4\pi M_s^2) \frac{\partial F\left(\frac{2r_o}{h}\right)}{\partial\left(\frac{2r_o}{h}\right)}\right](\Delta r_o)^2 \\ & + \frac{1}{2}\sum_{n=1}^{\infty}\left\{\frac{\pi}{r_o} h\sigma_w n^2 + 2\pi h M_s (H - H_o) - (2\pi h)(4\pi M_s^2) \frac{\partial F\left(\frac{2r_o}{h}\right)}{\partial\left(\frac{2r_o}{h}\right)}\right. \\ & \left. + h(4\pi M_s^2) \frac{2r_o}{h}\left[L_n\left(\left(\frac{2r_o}{h}\right)^2\right) - L_n(0)\right]\right\}(\Delta r_n)^2 \end{aligned}$$

$$
\begin{aligned}
&- \left[2\pi r_o^2 h M_s H_1 \cos\theta_1\right](\Delta r_1) \\
&- \frac{1}{2}\left[8\pi r_o h M_s H_1 \cos\theta_1\right](\Delta r_1)(\Delta r_o) \\
&- \frac{1}{2}\sum_{n=1}^{\infty}\sum_{m=1}^{\infty}\{[2\pi r_o h M_s H_1 \delta_{n,m\pm1}\cos(n\theta_n - m\theta_m)](\Delta r_n)(\Delta r_m) \\
&\quad - (2\pi r_o^2 h M_s H_1 \delta_{n1}\delta_{m1}\sin\theta_1)(\Delta r_n)(\Delta\theta_m)\} \\
&- \left[2\pi r_o^3 h M_s H_2 \cos 2\theta_2\right](\Delta r_2) \\
&- \frac{1}{2}\left[12\pi r_o^2 h M_s H_2 \cos 2\theta_2\right](\Delta r_o)(\Delta r_2) \\
&- \frac{1}{2}\sum_{n=1}^{\infty}\sum_{m=1}^{\infty}\{[3\pi r_o^2 h M_s H_2(\delta_{n1}\delta_{m1}\cos 2\theta_1 + \delta_{n,m\pm2}\cos(n\theta_n - m\theta_m))] \\
&\quad (\Delta r_n)(\Delta r_m) - 2\pi r_o^3 h M_s H_2 \delta_{n2}\delta_{m2} n \sin 2\theta_2](\Delta r_n)(\Delta\theta_m)\}
\end{aligned}
\tag{27}
$$

By inspection of Equation 27, it is appropriate to note the significance of some of the terms. The term $-\partial[\Delta r_1(\partial E_H^1/\partial r_1)_o]/\partial\theta_1 = -\Delta r_1(\partial^2 E_H^1/\partial r_1\partial\theta_1)_o$ is a torque tending to turn a domain into the direction in which the force tending to move the domain is most positive. On the other hand, the term $-\partial[\Delta r_2(\partial E_H^2/\partial r_2)_o]/\partial\theta_2 = -\Delta r_2(\partial^2 E_H^2/\partial r_2\partial\theta_2)_o$ is a torque tending to turn a domain into the direction in which the force tending to deform the domain is most positive.

2. Bubble domain dissipation

The preceding section treated forces arising from the total energy variation of the system. In order to set up equations for translation,

size change, and deformation of domains, it is necessary to add a kinetic energy term to the other energy terms and to add a term accounting for the domain dissipation as the wall moves. The "wall mass" is negligibly small in practical cases, so that the kinetic energy term may be ignored and the domain dynamics may be proceeded to the matter of dissipation. The method used to take dissipative effects into account is to compute the power dissipation produced by a general variation in domain shape using the wall dissipation equation and then to set this equal to the power produced by the variation.

Wall motion in many magnetic materials is describable in terms of a wall motion coercivity and a wall motion mobility. In some ferrites, there exists a linear relationship between wall velocity and drive field provided that the drive field is sufficiently low (32, 33). In uniaxial hexagonal ferrites, such as barium ferrite, the wall velocity is a non-linear function of drive field (34). On the other hand, orthoferrites and garnets are characterized by a linear relationship between wall velocity and drive field (22). However, it will be assumed here that each segment of 180° domain wall in bubble materials has the velocity-drive field relation,

$$|v_n| = \begin{cases} \mu_w(|H_z| - H_c) & , \quad |H_z| > H_c \\ 0 & , \quad |H_z| \leq H_c \end{cases} \tag{28}$$

where v_n is the local wall velocity in a direction normal to the wall, H_z is the total local field component parallel to the magnetization, H_c is the wall motion coercivity, and μ_w is the wall mobility.

Consider now a portion of the domain wall as shown in Figure 1 with the applied local field, H_z, which is positive when it lies in the positive z direction. The power input per unit area from the local field to an inward moving (decreasing r_b) segment of the domain wall is independent of the details of the magnetic configuration within the wall and is

$$p_{in} = 2 M_s |H_z||v_n| \tag{29}$$

Since the "wall mass" has been assumed to be negligible, the wall inertial effects can be disregarded in evaluation of power output. Therefore, the power input must be equal to the power dissipated per unit wall area. Eliminating H_z in Equation 29 from Equation 28 results in

$$p_{diss} = 2 M_s (H_c |v_n| + \frac{1}{\mu_w} v_n^2) \tag{30}$$

It will be assumed that the wall coercivity is uniform over the wall and is independent of the direction of wall motion. Thus in evaluation of total domain wall dissipation, H_c is considered as a constant force opposing the motion at each segment of domain wall. The total domain dissipation can be obtained by integrating the dissipation density over the domain area,

$$P_{diss} = \int_{wall} 2M_s (H_c |v_n| + \frac{1}{\mu_w} v_n^2) \, da \tag{31}$$

where da is the differential wall area. Since for a circular domain,

$$v_n = \vec{i}_r \cdot \vec{v}_d \tag{32}$$

where $\vec{i}_r$ is the unit vector in the radial direction and $\vec{v}_d$ is the velocity of the domain, Equation 31 becomes

$$P_{diss} = 2hM_s \int_0^{2\pi} (H_c|\vec{v}_d\cdot\vec{i}_r| + \frac{1}{\mu_w}|\vec{v}_d\cdot\vec{i}_r|^2) r_b(\theta)d\theta \tag{33}$$

Setting $r_b(\theta) = r_o$ yields

$$P_{diss} = 2hr_oM_s \int_0^{2\pi} (H_c|\vec{v}_d\cdot\vec{i}_r| + \frac{1}{\mu_w}|\vec{v}_d\cdot\vec{i}_r|^2)d\theta \tag{34}$$

Now for a circular domain,

$$\vec{v}_d \cdot \vec{i}_r = \frac{dr_b(\theta)}{dt}$$

$$= \sum_{n=0}^{\infty} \left[\left(\frac{\partial r_b(\theta)}{\partial \Delta r_n}\right)_o \frac{d\Delta r_n}{dt} + \left(\frac{\partial r_b(\theta)}{\partial \Delta \theta_n}\right)_o \frac{\partial \Delta\theta_n}{dt} \right]$$

$$= \sum_{n=0}^{\infty} \cos[n(\theta - \theta_n)] \frac{d\Delta r_n}{dt} \tag{35}$$

Substituting Equation 35 into Equation 34 and carrying out the integration yield

$$P_{diss} = 4\pi r_o hM_s \left\{H_c \left[\left|\frac{d\Delta r_o}{dt}\right| + \frac{2}{\pi}\sum_{n=1}^{\infty}\left|\frac{d\Delta r_n}{dt}\right|\right]\right.$$

$$\left. + \frac{1}{\mu_w}\left[\left(\frac{d\Delta r_o}{dt}\right)^2 + \frac{1}{2}\sum_{n=1}^{\infty}\left(\frac{d\Delta r_n}{dt}\right)^2\right]\right\} \tag{36}$$

Equation 36 shows that there are two characteristic types of dissipation: one contribution is proportional to the square of the wall velocity, and one contribution is proportional to the absolute value of the wall velocity. These can be understood physically. In one form of dissipation the

dissipative drag force which acts on the wall is proportional to the wall velocity. The rate of energy loss is equal to this force times the velocity and is, therefore, proportional to the square of the velocity. The second type of dissipation involves a fixed loss energy per unit distance of wall travel, independent of velocity. The amount of energy given up by the wall is proportional to the displacement of the wall, so that the power loss is proportional to the wall velocity. The proportional constants for these two types are related to wall mobility and coercivity, respectively.

3. Bubble domain velocity

As stated in the preceding sections, a bubble domain may propagate when a field gradient is applied. In the case of a uniform gradient, motion of a bubble may have a constant velocity. When the applied field gradient is nonuniform as in the most practical cases, the response will be complex and could have nonuniform domain velocity and change in domain size and shape. These can be analyzed by taking dissipative processes into account to set the sum of the power dissipation, Equation 36, and the rate of energy change from variation, Equation 27, equal to zero.

The domain radius function, Equation 2, describes the domain shape in the plane of the platelet. The Δr_n and $\Delta\theta_n$ describe small variations from a circular domain of radius $r_b(\theta) = r_o$. Each individual variation of Δr_n has different effect on domain. Figure 5 shows the schematic diagram for domain shape variations by Δr_n from n=0 to n=3. It can be seen clearly that from the point of view of the total domain, Δr_o variation

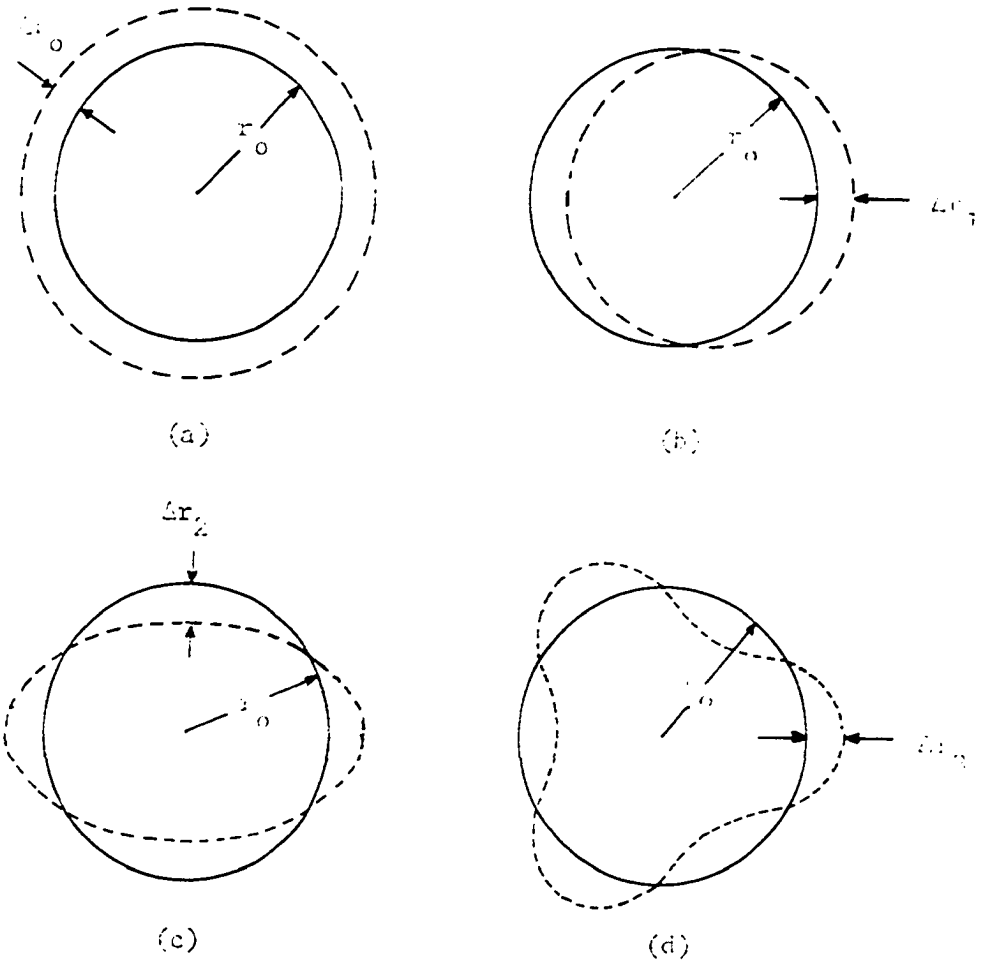

Figure 5. Schematic diagram for domain variations by (a) Δr_0, (b) Δr_1, (c) Δr_2, (d) Δr_3

accounts for change in domain size and Δr_1 variation accounts for translation of domain while Δr_n's for $n \geq 2$ account for deformation of domain shape, specifically Δr_2 for elliptical shape variation. In this section, translation of domain will be discussed and change in size and shape will be discussed in the next two sections.

Consider now an initially circular domain in which only $d\Delta r_1/dt$ is nonzero. In this case, the rate of energy change from Equation 27 becomes,

$$\frac{dE_T}{dt} = \frac{dE_T}{d\Delta r_1} \frac{d\Delta r_1}{dt}$$

$$= - 2\pi r_o^2 h M_s H_1 \frac{d\Delta r_1}{dt} \tag{37}$$

In Equation 37, the second order terms including the coupling terms have been neglected under the condition of Equation 3 in order to evaluate the absolute value of domain velocity. Also evaluation has been considered in the direction of which the domain velocity is maximum ($\theta_1 = 0$) because there exists a torque to turn the domain into this direction as mentioned before. Setting the sum of Equation 37 and the power dissipation, Equation 36, due to $d\Delta r_1/dt$ equal to zero yields

$$4\pi r_o h M_s \left[\frac{2H_c}{\pi} \left|\frac{d\Delta r_1}{dt}\right| + \frac{1}{2\mu_w} \left(\frac{d\Delta r_1}{dt}\right)^2 \right]$$

$$- 2\pi r_o^2 h M_s H_1 \left|\frac{d\Delta r_1}{dt}\right| = 0 \tag{38}$$

The driving field of which the magnitude is defined by

$$\Delta H_1 = 2r_o H_1 \tag{39}$$

orientates in the direction in which the bias decreases most rapidly, i.e., in the positive x direction according to Equation 14. In fact, ΔH_1 is the maximum field difference across the circular domain due to linear gradient field. Thus, Equation 38 becomes,

$$4\left(\frac{2H_c}{\pi} + \frac{1}{2\mu_w}\left|\frac{d\Delta r_1}{dt}\right|\right) - \Delta H_1 = 0 \tag{40}$$

A variation in Δr_1 can be identified with

$$|v_d| = \left|\frac{d\Delta r_1}{dt}\right| \tag{41}$$

where v_d is the circular domain propagating velocity. Consequently, Equation 40 implies

$$|v_d| = \frac{r_w}{2}\left(\Delta H_1 - \frac{8}{\pi} H_c\right), \quad \Delta H_1 > \frac{8}{\pi} H_c \tag{42a}$$

$$|v_d| = 0, \quad \Delta H_1 \leq \frac{8}{\pi} H_c \tag{42b}$$

This shows that in order to have a bubble domain in motion, the driving field, ΔH_1, has to be larger than $(8/\pi)H_c$. The domain will propagate in the direction in which the bias field decreases most rapidly. Comparison of Equation 28 and 42 shows that it is possible to define a domain mobility and coercivity in terms of the wall mobility and coercivity as

$$\mu_d = \frac{1}{2}\mu_w \tag{43}$$

$$H_{cd} = \frac{8}{\pi} H_c \tag{44}$$

if ΔH_1 is taken to be the drive field.

Equation 42 has been used to calculate the bubble domain velocity (5-9) when a uniform field gradient is applied. In the case of non-uniform gradient, caution has to be taken in using Equation 42 to compute the domain velocity. As defined in Equation 14, the magnitude of the applied field may change as the domain moves because the coordinate system of the applied field follows the center of the circular domain. Consequently, the magnitude of the drive field may change as the domain propagates, so that the domain velocity varies along the propagation channel. In order to calculate the domain velocity under nonuniform field gradient it will be necessary to know the variation of the applied field along the propagation channel.

4. Bubble domain size

The domain size variation will be considered in two cases. First the equilibrium size of stable domain can be determined by using the general force Equation 9 with the total applied field. On the other hand, small variation in domain size from equilibrium can be determined by using the radial stability functions. The same dissipation function may be used in both cases.

For the first case, setting all the $d\Delta r_n/dt$ except $d\Delta r_o/dt$ equal to zero in Equation 36 yields the dissipation produced by a size change

$$P_{diss} = 4\pi r_o h M_s \left[\pm H_c + \frac{1}{\mu_w} \frac{d\Delta r_o}{dt} \right] \frac{d\Delta r_o}{dt} \tag{45}$$

where the upper sign in front of H_c is for an expanding domain. The rate of energy change due to Δr_o in Equation 27 is

$$\frac{dE_T}{dt} = 4(2\pi M_s^2)(\pi h^2)\left[\frac{\ell}{h} + \frac{d}{h}\frac{H-H_o}{4\pi M_s} - F\left(\frac{d}{h}\right)\right]\frac{d\Delta r_o}{dt} \qquad (46)$$

Setting the sum of Equations 45 and 46 equal to zero yields the equation for determining the domain diameter

$$-\frac{h}{2\mu_w(4\pi M_s)}\frac{d}{h}\frac{d\left(\frac{d}{h}\right)}{dt} = \frac{\ell}{h} + \frac{d}{h}\frac{H-H_o\pm H_c}{4\pi M_s} - F\left(\frac{d}{h}\right) \qquad (47)$$

where $d(d) = 2d(r_o) = 2d(\Delta r_o)$. This differential equation thus shows that the domain diameter relaxes toward a value which is the solution to the general force equation as in the static case, Equation 9, except that H has been replaced by a composite bias field, $H-H_o\pm H_c$. The bias field, $H-H_o$, determines the equilibrium domain diameters, the stable and the unstable ones, for zero coercivity. Now since the sign of $\pm H_c$ must be determined in each case, there is a small continuous range of stable solutions about both the stable and unstable diameters. In other words, coercivity produces two stable range of solutions rather than one stable solution point and one unstable solution point. The large diameter solutions to the force equation for $H-H_o+H_c$ and $H-H_o-H_c$ bound the solution range which brackets the zero coercivity stable solution and similarly the small solutions to the force equation for $H-H_o+H_c$ and $H-H_o-H_c$ bound the solution range which brackets the zero coercivity unstable solution. Figure 6 shows an example of solutions to the force equation in the presence of coercivity. P and Q represent the stable and unstable solutions for zero coercivity, respectively. The large diameter solutions for $H-H_o+H_c$ and $H-H_o-H_c$ are marked P_+ and P_-, respectively, while the small

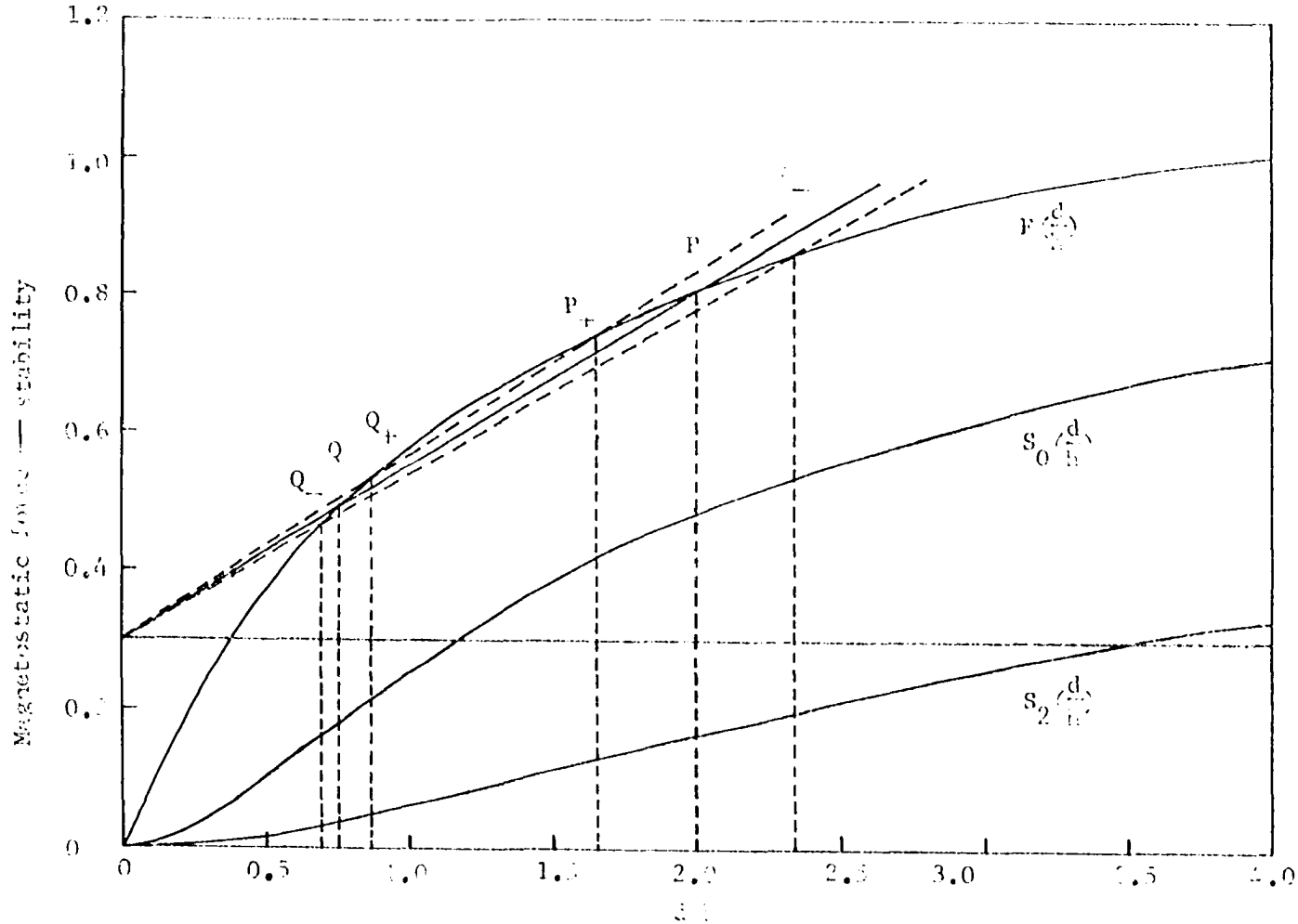

Figure 4. Solutions of stable diameter to the force equation in the presence of coercivity

diameter solutions for $H-H_o+H_c$ and $H-H_o-H_c$ are marked Q_+ and Q_-, respectively. Coercivity stabilizes domains having diameter between P_+ and P_- and between Q_+ and Q_-. Small diameter coercivity stabilized solutions have been observed in the process of carrying out the mobility measurement (22, 35).

For the second case, the energy variation expression, Equation 27, may be considered as an expansion of energy about the domain diameter which is the solution to the force equation. Consequently, the rate of energy change using Equation 27 and neglecting the coupling terms is

$$\frac{dE_T}{dt} = \frac{\partial E_T}{\partial \Delta r_o} \frac{d\Delta r_o}{dt}$$

$$= -8\pi h(2\pi M_s^2) \frac{h}{d} \left[\frac{\ell}{h} - S_o\left(\frac{d}{h}\right) \right] \Delta r_o \frac{d\Delta r_o}{dt} \tag{48}$$

Using the same procedures by setting the sum of Equations 45 and 48 equal to zero yields

$$\frac{1}{\mu_w(4\pi M_s)} \frac{d\Delta r_o}{dt} = \left(\frac{h}{d}\right)\left[\frac{\ell}{h} - S_o\left(\frac{d}{h}\right) \right] \frac{\Delta r_o}{r_o} \mp \frac{H_c}{4\pi M_s} \tag{49}$$

Thus the domain radius relaxes towards

$$\left| \frac{\Delta r_o}{r_o} \right| = \frac{H_c}{4\pi M_s} \left| \frac{\frac{d}{h}}{\frac{\ell}{h} - S_o\left(\frac{d}{h}\right)} \right| \tag{50}$$

Therefore, coercivity stabilizes the domain for departures in radius from equilibrium up to this value. Defined by the usual time factor, $\exp(-t/\tau)$, the relaxation time is

$$\tau = - \frac{r_o}{\mu_w 4\pi M_s} \frac{\frac{d}{h}}{\frac{\ell}{h} - S_o(\frac{d}{h})} \tag{51}$$

Equation 50 may be used to limit the magnitude of coercivity for a domain to have a defined variation range. As in the first case, the diameters bounding the solution range bracketing the zero coercivity solutions may also be computed by Equation 50.

5. Bubble domain shape variation

The domain shape variation in the presence of dissipative processes can be considered by Δr_n variation for $n \geq 2$. The applied field discussed has been considered only up to the second order term. Also to characterize the effect of coercivity in limiting the attainment of stable movable cylindrical domains it is necessary only to consider the elliptical shape variation mode (n=2) in addition to the size (n=0) and translation (n=1) modes (7, 30). Thus, only the elliptical shape variation will be considered here. For higher order modes, the similar procedures can be applied.

The power dissipation produced by the elliptical shape variation is from Equation 36

$$P_{diss} = 4\pi r_o h M_s [\pm \frac{2}{\pi} H_c + \frac{1}{2\mu_w} \frac{d\Delta r_2}{dt}] \frac{d\Delta r_2}{dt} \tag{52}$$

where the upper sign is for positive $d\Delta r_2/dt$. The rate of change of domain energy due to Δr_2, again negleting the coupling terms, is from Equation 27

$$\frac{dE_T}{dt} = \frac{\partial E_T}{\partial \Delta r_2} \frac{d\Delta r_2}{dt}$$

$$= 12\pi h(2\pi M_s^2)\left(\frac{h}{d}\right)\left[\frac{\ell}{h} - S_2\left(\frac{d}{h}\right)\right]\Delta r_2 \frac{d\Delta r_2}{dt}$$

$$\pm \pi r_o^3 h M_s H_2 \frac{d\Delta r_2}{dt} \qquad (53)$$

where the term produced by H_2 has been computed in the direction in which the domain is most elliptical ($\theta_2 = 0$ and $\theta_2 = 90^\circ$). The upper sign is for positive $d\Delta r_2/dt$ ($\theta_2 = 0$), while the lower sign is for negative $d\Delta r_2/dt$ ($\theta_2 = 90^\circ$). Defining

$$\Delta H_2 = 2r_o^2 H_2 \qquad (54)$$

and setting the sum of Equations 52 and 53 equal to zero yield

$$-\frac{1}{\mu_w 4\pi M_s}\frac{d\Delta r_2}{dt} = 3\left(\frac{h}{d}\right)\left[\frac{\ell}{h} - S_2\left(\frac{d}{h}\right)\right]\frac{\Delta r_2}{r_o} \mp \frac{\Delta H_2}{8\pi M_s}$$

$$\pm \frac{4}{\pi}\frac{H_c}{4\pi M_s} \qquad (55)$$

For both cases, positive and negative $d\Delta r_2/dt$, the domain shape variation amplitude thus relaxes towards

$$\left|\frac{\Delta r_2}{r_o}\right| = \left|\frac{\Delta H_2}{8\pi M_s} \mp \frac{4}{\pi}\frac{H_c}{4\pi M_s}\right| \left|\frac{1}{3\left(\frac{h}{d}\right)\left[\frac{\ell}{h} - S_2\left(\frac{d}{h}\right)\right]}\right| \qquad (56)$$

The relaxation time is

$$\tau = \frac{r_o}{\mu_w 4\pi M_s}\frac{1}{3\left(\frac{h}{d}\right)\left[\frac{\ell}{h} - S_2\left(\frac{d}{h}\right)\right]} \qquad (57)$$

ΔH_2 is the maximum field difference on the circular domain wall due to the applied second order field. This drive field causes the initially circular domain to become elliptical as shown in Figure 5c. The ratio of the difference in ellipse semiaxes to their average, $2\Delta r_2/r_o$, can be computed by using Equation 56. It can be seen from Equation 56 that coercivity stabilizes the domain for variation amplitude due to the second order field up to this value. In practical materials, H_c is small for keeping velocity high. Consequently, in device applications, it is necessary to keep the nonlinear term of the applied field as small as possible in order to avoid false information.

6. Discussions

The preceding sections have discussed the dynamics of the magnetic bubble domains under the nonuniform applied field. With the applied field of Equation 14, three modes of motion including size change (n=0), translation (n=1) and elliptical shape variation (n=2) have been discussed separately in the presence of dissipative processes. These provide some general and simplified picture of propagation of bubble domains. It will be emphasized here that the domain has been considered initially in circular shape. All the parameters used and defined previously are on the basis of initial domain radius, r_o. As noted before, the domain will propagate in the direction in which the gradient is maximum and will move to the place where the total energy is minimum. During the propagation, the domain may change its size and shape in addition to translation. Under the assumption that these variations are sufficiently small compared to

the domain diameter, the energy expression remains valid at any point of the propagation channel. Consequently, all the previous discussions may be applied locally provided that the drive field varies along the propagation channel. Under nonuniform field gradient, the translational velocity of domains, unlike the uniform case, will not be constant and its magnitude depends on the variation of the applied field.

The second variation of the energy with respect to Δr_n and $\Delta\theta_n$ determines the stability of the domain. Since the stiffness of the domain with respect to externally applied forces is proportional to the coefficient of the bilinear form which is the second variation of the energy, the matrix formed by these coefficients is called the stiffness matrix (7). The stiffness matrix is composed of three independent submatrices: radial, angular, and mixed stiffness matrices. Inspection of Equation 27 shows that with nonuniform applied field there are two kinds of stiffness matrices, radial and mixed. Unlike the static case, the radial stiffness matrix consists of off-diagonal elements in addition to diagonal elements. Since the mixed stiffness matrix exists, the system is not completely metastable with respect to angle. The preceding analysis of domain size change, shape deformation, and domain translation has neglected the coupling terms which is the off-diagonal elements of the radial stiffness matrix under the assumption that Δr_n variations are sufficiently small compared to the equilibrium domain radius. Also it was considered on the basis of local evaluation so that the previous analysis may still be applied at any point along the propagation channel. If all the coupling terms are included, the analysis will be much more complicate.

The crudest approximation in the previous analysis, however, comes from wall coercivity, H_c. In calculation of the total domain dissipation, the wall coercivity was considered to have the same magnitude and the same velocity-drive field relation, Equation 28, at each segment of domain wall. In most magnetic materials, coercivity is never uniform and in many cases depends on the direction of wall motion (30). Also H_c varies as wall moves (32). Consequently, the total domain dissipation, Equation 36, should include the nonlinear coercivity coupling terms which appears even in the lowest order. The nonlinear coupling terms tend in general to couple in additional modes even if only one $d\Delta r_n/dt$ is nonzero. Thus, Equations 49 and 55 become rather crude approximation because nonuniform coercivity introduces nonlinear mode coupling. In device application, the most important factor is the domain propagation velocity. Equation 42 provides the domain velocity-drive field relation. Measurements on a number of orthoferrites (28) showed that the linear relation can be applied approximately for large drive fields using dynamic coercivity instead of the domain coercivity defined in Equation 44. The magnitude of dynamic coercivity is appreciably higher than H_{cd} and depends on materials and treatments of materials. Nonetheless, the discussion of the effects of dissipative processes in terms of dissipation equations accounts correctly for the effects of coercivity to lowest order without being required to examine the coupling of modes or the origins of coercivity. The results obtained do provide a general picture of the dependence of the effect of coercivity on the various domain parameters.

C. Analysis of Bubble Domain Permalloy Propagating Circuit

1. Calculation of magnetic field produced by permalloy bars in the propagating circuit

The cylindrical magnetic domain will propagate, if a highly localized gradient field is applied. Such field can be produced by current-carrying small conductor loops (6, 36, 37) or by isotropic permaloy overlay magnetized by applying transverse magnetic field (6, 9). The simplest and easiest way, however, to manipulate domains is to use permalloy overlay circuit. Even in a current drive propagating circuit, an array of permalloy dots is used to introduce an asymmetry into the pattern (36, 37). The transverse magnetic field applied to magnetize permalloy overlay has no direct effect on the domains due to high uniaxial anisotropy of the platelet materials. Thus the induced magnetic poles on permalloy bars provide a local field gradient to move domains.

There are two general classes of permalloy circuit used in manipulation of domains. The first class, the angelfish circuit, utilizes the fact that a cylindrical domain can be modulated in size by increasing or decreasing the bias field. With domain in and out of asymmetrical energy traps created by wedge-shaped permalloy films, bubble domain motion is achieved. The most common and effective way, however, is the second method of propagation. An in-plane rotating field acting on a structured permalloy pattern generates traveling positive and negative poles to selectively attract and repel and thereby control the motion of a cylindrical domain. One commonly used suitable pattern is the T-bar structure (6, 9). Recently, an alternative circuit element, the Y-bar,

has been proposed and developed (38). One major advantage in the operation of Y-bar is that the Y-bar arrangement has four stable positions of about equal pole strength. The T-bar, on the other hand, lacks a well-localized pole position in the center of the T. For this reason, Y-bar might provide a speed advantage.

Consider now a pattern of T-bar structure for straight line propagation of cylindrical domains. Figure 7 shows one complete cycle of domain propagation from position A to position E and the corresponding directions of the applied transverse rotating field. If the transverse field is applied along the long dimension of a bar, the demagnetizing field of the bar is minimal and strong magnetic poles are formed at the ends of the bars. If the transverse field is applied across the short dimension of a bar, the large demagnetizing effect opposes formation of any appreciable pole strength. Thus the magnetic poles attracting or repelling cylindrical domains provide a local field gradient to fulfill domain motion. To complete one cycle of motion, it requires four steps of jump, A-B, B-C, C-D, and D-E, as shown in Figure 7. It, however, can be classified into two categories, A-B, C-D, and B-C, D-E, if the magnetic poles induced in the permalloy bars by the field from the domain are neglected. Each period needs two of each type of step. In the following, field produced in each type will be computed.

Consider first the propagation of a domain from the center to the end of the T-bar, A-B in Figure 7. Figure 8 shows both top and side views of the configuration and the coordinate system from which the field will be calculated. The origin of the coordinate system is at the

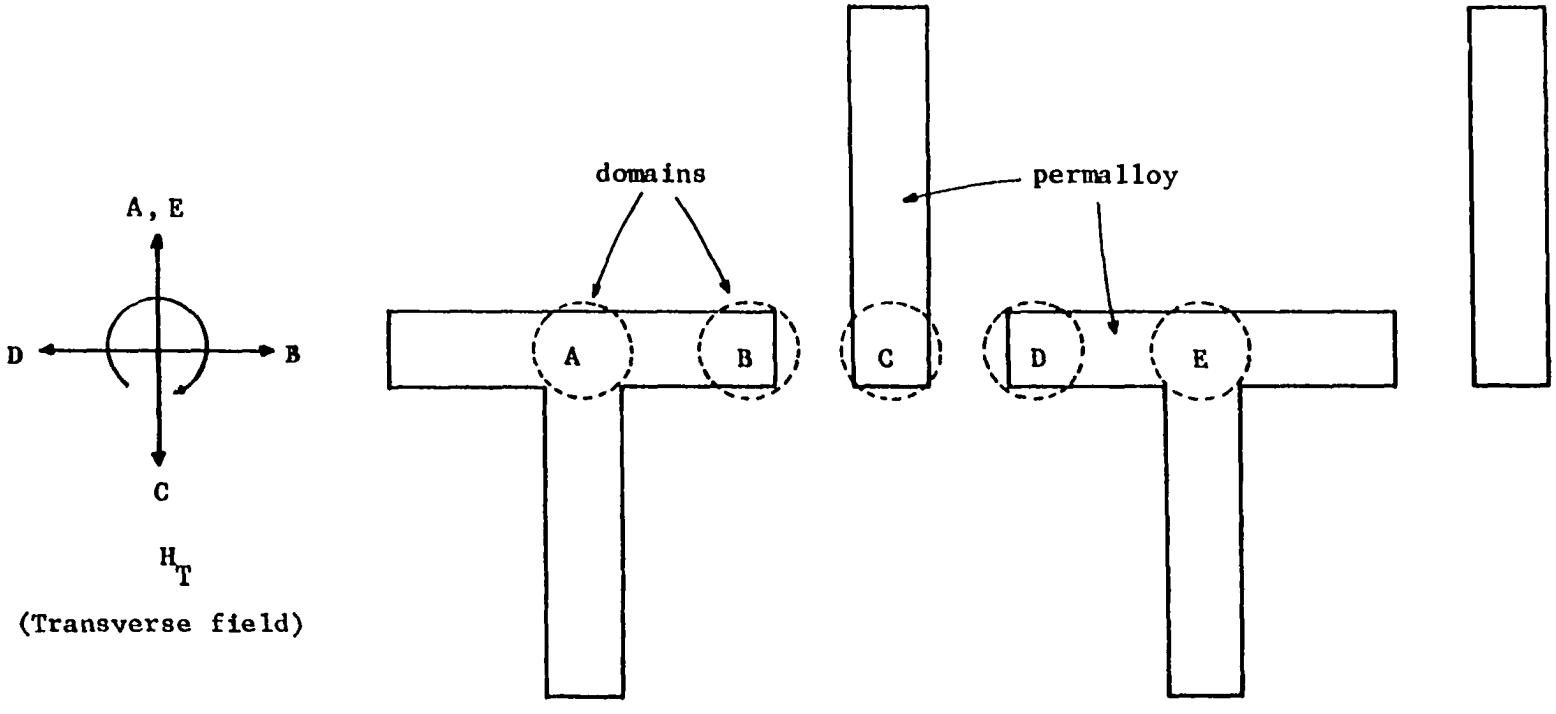

Figure 7. Schematic diagram showing one complete cycle of domain propagation with the directions of corresponding transverse rotating field

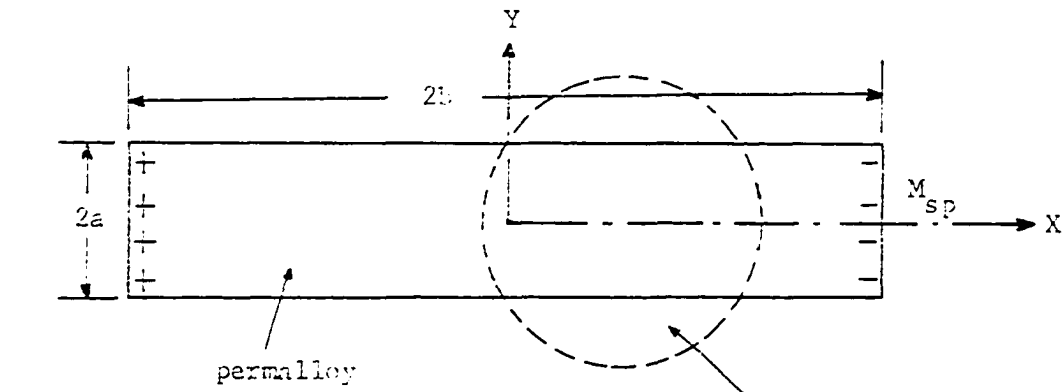

(a) Top view

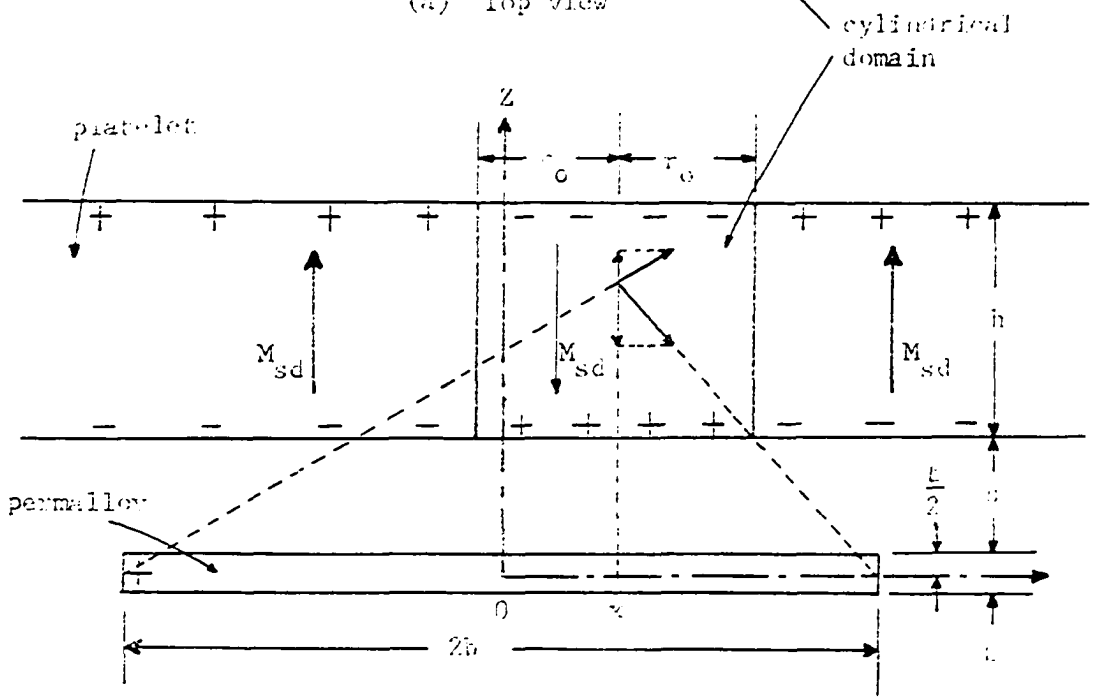

(b) Side view

Figure 8. Schematic diagram for calculation of magnetic field (A-B)

center of T-bar. Magnetic pole strength induced at the ends of the bar is denoted by M_{sp} to distinguish it from the saturation magnetization of domain M_{sd}. To simplify the calculation, the magnetic field will be computed at the center of the domain along the x direction instead of two dimensional field. For high uniaxial anisotropy of domain material, only the z-component of the magnetic field is of interest here. Under the assumption of cylindrical domain walls (no bulging) the magnetic field at any x acting on the domain may be evaluated by z-component of its average value over the platelet thickness, h. Thus,

$$\bar{H} = \frac{1}{h} \int_0^h H_z(z)dz \tag{58}$$

This, in fact, is the difference in scalar magnetic potential between the top and the bottom surfaces of the platelet. Although it consists of many repeated pattern of Figure 7 in actual devices, only the field produced by the nearest neighboring magnetic poles will be considered here as in Figure 8.

Since the thickness of the permalloy overlay usually is negligibly small compared to the other dimensions, the magnetic pole strength at the ends of the bar will be considered to be concentrated at z=0. Thus, the z-component magnetic field at any x average over the platelet thickness will be

$$\bar{H}_{A-B} = \frac{1}{h}\int_{s+\frac{t}{2}}^{s+\frac{t}{2}+h} dz \left\{ \int_{-a}^{a} \frac{M_{sp}t}{\left[y^2+z^2+(b+x)^2\right]} \frac{zdy}{\left[y^2+z^2+(b+x)^2\right]^{\frac{1}{2}}} \right.$$

$$\left. - \int_{-a}^{a} \frac{M_{sp}t}{\left[y^2+z^2+(b-x)^2\right]} \frac{zdy}{\left[y^2+z^2+(b-x)^2\right]^{\frac{1}{2}}} \right\} \qquad (59)$$

Exchanging the integrals and integrating over z yield

$$\bar{H}_{A-B} = \frac{M_{sp}t}{h}\int_{-a}^{a} dy \left\{ \frac{1}{\left[y^2+(b+x)^2+(s+\frac{t}{2})^2\right]^{\frac{1}{2}}} - \frac{1}{\left[y^2+(b+x)^2+(s+\frac{t}{2}+h)^2\right]^{\frac{1}{2}}} \right.$$

$$\left. + \frac{1}{\left[y^2+(b-x)^2+(s+\frac{t}{2}+h)^2\right]^{\frac{1}{2}}} - \frac{1}{\left[y^2+(b-x)^2+(s+\frac{t}{2})^2\right]^{\frac{1}{2}}} \right\} \qquad (60)$$

Integrating over y results in

$$\bar{H}_{A-B} = \frac{M_{sp}t}{h} \ell n \left\{ \frac{\left[a+\sqrt{a^2+(b+x)^2+(s+\frac{t}{2})^2}\right]\left[-a+\sqrt{a^2+(b+x)^2+(s+\frac{t}{2}+h)^2}\right]}{\left[-a+\sqrt{a^2+(b+x)^2+(s+\frac{t}{2})^2}\right]\left[a+\sqrt{a^2+(b+x)^2+(s+\frac{t}{2}+h)^2}\right]} \right.$$

$$\left. \frac{\left[a+\sqrt{a^2+(b-x)^2+(s+\frac{t}{2}+h)^2}\right]\left[-a+\sqrt{a^2+(b-x)^2+(s+\frac{t}{2})^2}\right]}{\left[-a+\sqrt{a^2+(b-x)^2+(s+\frac{t}{2}+h)^2}\right]\left[a+\sqrt{a^2+(b-x)^2+(s+\frac{t}{2})^2}\right]} \right\} \qquad (61)$$

Similar calculation can be used for the second case from the end of the T-bar to the end of the neighboring bar, B-C in Figure 7. As shown in Figure 9, the magnetic poles induced at the T-bar will be assumed to be concentrated at the top of the center bar. For convenience, only x-dependent field will be computed. Thus, the z-component magnetic field at any x average over the platelet thickness in this case will be

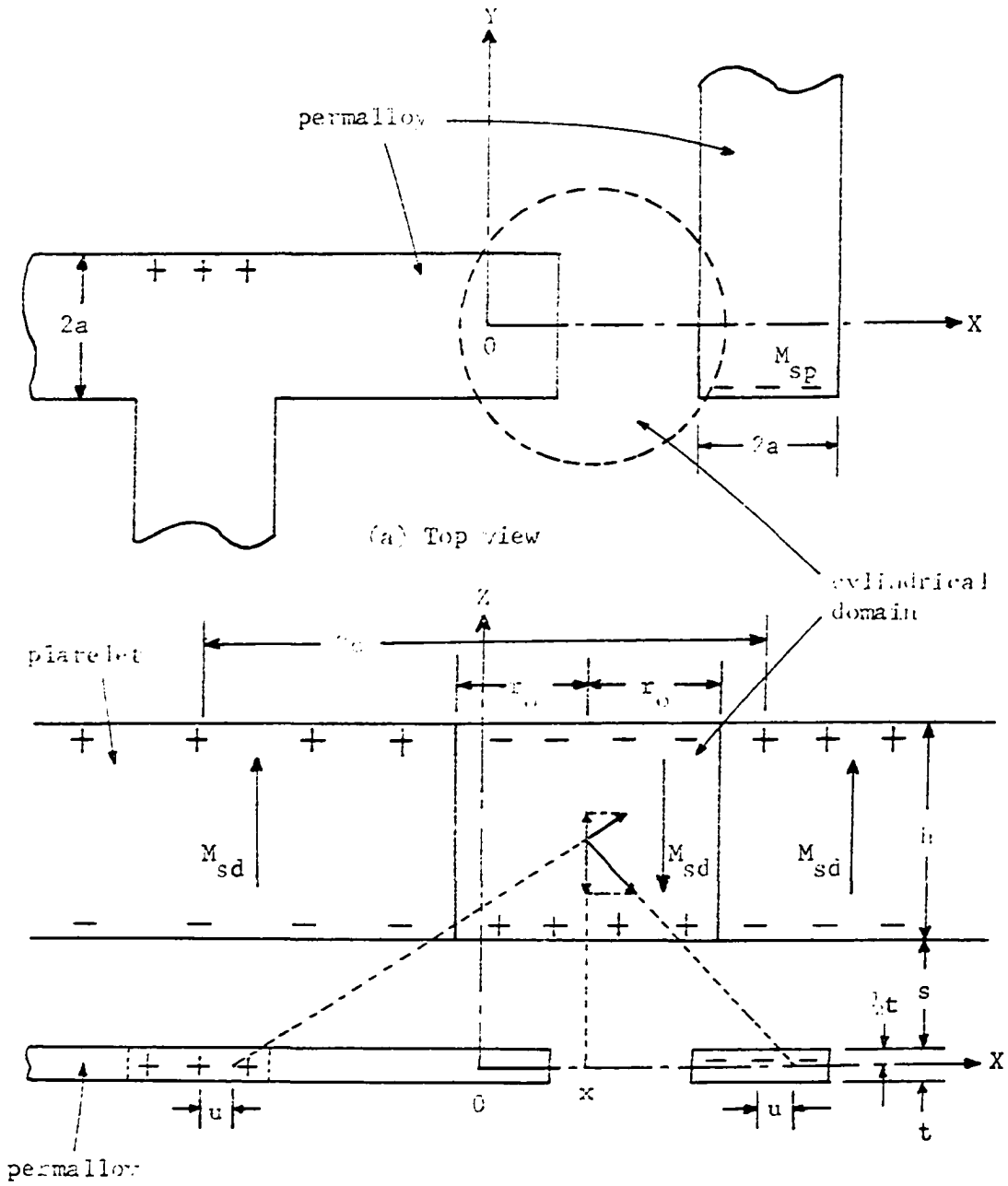

Figure 9. Schematic diagram for calculation of magnetic field (3-C)

$$\bar{H}_{B-C} = \frac{1}{h}\int_{s+\frac{t}{2}}^{s+\frac{t}{2}+h} dz \left\{ \int_{-a}^{a} \frac{M_{sp}\, t\, z\, du}{\left[(c+x-u)^2+a^2+z^2\right]^{3/2}} \right.$$

$$\left. - \int_{-a}^{a} \frac{M_{sp}\, t\, z\, du}{\left[(c-x+u)^2+a^2+z^2\right]^{3/2}} \right\} \tag{62}$$

Exchanging the integrals and integrating over z yield

$$\bar{H}_{B-C} = \frac{M_{sp}\, t}{h}\int_{-a}^{a} du \left\{ \frac{1}{\left[(c+x-u)^2+a^2+(s+\frac{t}{2})^2\right]^{\frac{1}{2}}} - \frac{1}{\left[(c+x-u)^2+a^2+(s+\frac{t}{2}+h)^2\right]^{\frac{1}{2}}} \right.$$

$$\left. + \frac{1}{\left[(c-x+u)^2+a^2+(s+\frac{t}{2}+h)^2\right]^{\frac{1}{2}}} - \frac{1}{\left[(c-x+u)^2+a^2+(s+\frac{t}{2})^2\right]^{\frac{1}{2}}} \right\} \tag{63}$$

Integrating over u results in

$$\bar{H}_{B-C} = \frac{M_{sp}\, t}{h} \ell n \left\{ \frac{\left[(c+x+a)+\sqrt{(c+x+a)^2+a^2+(s+\frac{t}{2})^2}\right]}{\left[(c+x-a)+\sqrt{(c+x-a)^2+a^2+(s+\frac{t}{2})^2}\right]} \right.$$

$$\frac{\left[(c+x-a)+\sqrt{(c+x-a)^2+a^2+(s+\frac{t}{2}+h)^2}\right]\left[(c-x+a)+\sqrt{(c-x+a)^2+a^2+(s+\frac{t}{2}+h)^2}\right]}{\left[(c+x+a)+\sqrt{(c+x+a)^2+a^2+(s+\frac{t}{2}+h)^2}\right]\left[(c-x-a)+\sqrt{(c-x-a)^2+a^2+(s+\frac{t}{2}+h)^2}\right]}$$

$$\left. \frac{\left[(c-x-a)+\sqrt{(c-x-a)^2+a^2+(s+\frac{t}{2})^2}\right]}{\left[(c-x+a)+\sqrt{(c-x+a)^2+a^2+(s+\frac{t}{2})^2}\right]} \right\} \tag{64}$$

Equations 61 and 64 provide an approximate solutions of simplified x-dependent z-component z-average magnetic field along the propagating channel. More complete forms are needed to solve the periodic pattern

of permalloy propagating circuit. However, these equations seem to be enough to characterize the behavior of the fields and also simplify the analysis of domain motion.

2. Analysis of domain motion in the permalloy circuit

With the applied fields of Equations 61 and 64, domain motion will be discussed in this section. As mentioned previously, the analysis of domain motion includes domain translation and change in domain size and shape. It has been assumed that the applied field has the form of Equation 14, so that in order to match this form Equations 61 and 64 will be expanded at any x_o by Taylor's series

$$f(x) = f(x_o) + \sum_{n=1}^{\infty} \frac{1}{n!} f^n(x_o)(x-x_o)^n \tag{65}$$

where f(x) represents either $\bar{H}_{A-B}$ or $\bar{H}_{B-C}$ because both have been considered to be functions of x only. By comparing Equations 14 and 65, the coefficients of Equation 14 can be identified at any x_o with

$$H_o = - f(x_o) \tag{66}$$

$$H_1 = - f'(x_o) \tag{67}$$

$$H_2 = - \frac{1}{4} f''(x_o) \tag{68}$$

In Equation 66, the r-dependent term has been disregarded because it simplifies the analysis and moreover, it is closer to fit the actual field produced by the permalloy bars.

The domain size is determined by the general force equation. Setting Equation 47 equal to zero yields the equilibrium domain diameter. Since

the direction of the magnetic field produced by the magnetized permalloy bars is opposite to the initially applied uniform bias field, the domain will expand during the propagation along the channel. Figure 10 and Figure 11 show the variation of H_o's for $\bar{H}_{A-B}$ and $\bar{H}_{B-C}$, respectively, for b=5a, c=4a, and s+t/2=0.1h. Since the field is dependent on the width of the permalloy bars, the variation for several values of the ratio of a to h is also shown in the figures. It can be seen that the domain diameter is increasing either from A to B or from B to C. For domain moving from A to B, it seems to have a drastic change in domain size when a domain is approaching B. It is undesirable to have the composite bias field below the strip-out field. Although Figure 10 shows that at the end, point B, the composite bias field may be below the strip-out field, it should be considered that the field beyond point B increases again and the average field for a domain is not the same as in the center of the domain. Consequently, the figure at both ends has less significance for the determination of domain size. The variation of the width of the permalloy bar with the ratio of a to b remaining the same shows that the larger the width, the smaller the change in size except at the end. For the case of domain moving from B to C, there is no drastic change in field at the end and the difference of change in size by the variation of width is smaller than the first case. It shows the same trend as in the first case for the change in size with the variation of the width. It is desirable to have change in domain size during the propagation as small as possible.

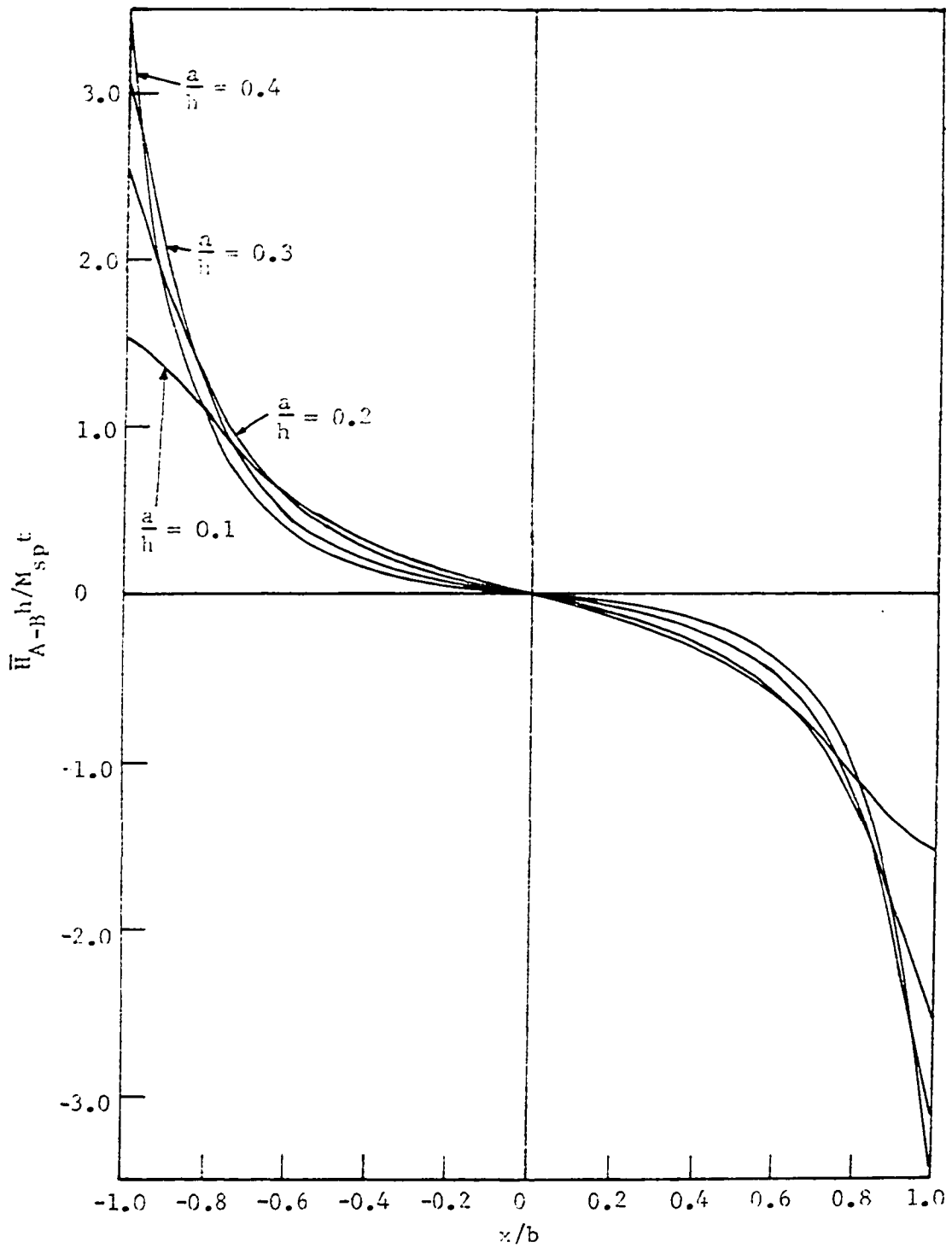

Figure 10. Variation of H_o for $\bar{H}_{A-B}$ along the channel

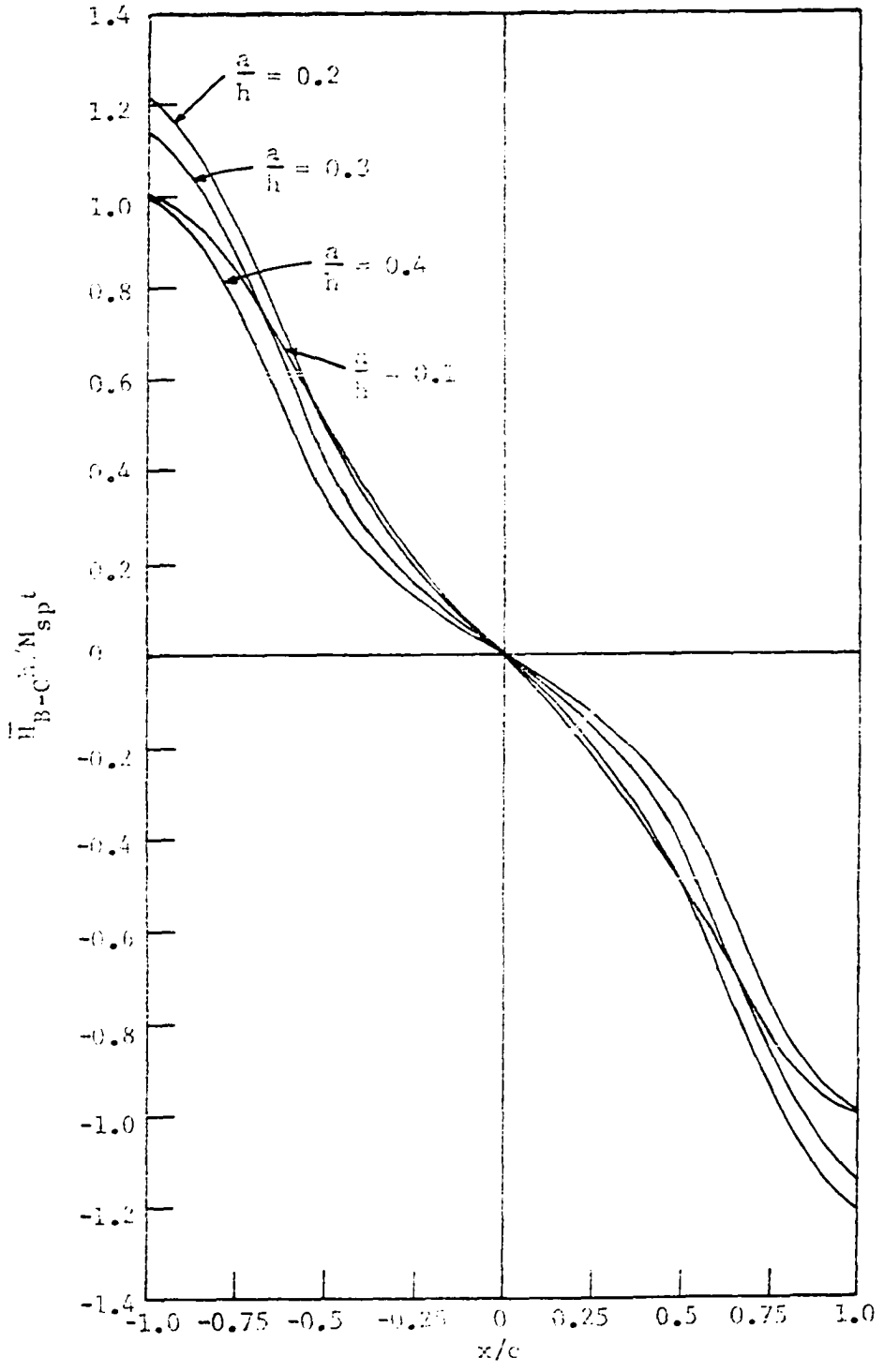

Figure 11. Variation of H_o for $\bar{H}_{B-C}$ along the channel

The most important factor in discussion of domain propagation is domain velocity. The absolute value of domain velocity has been defined in Equation 42. The driving field ΔH_1 must be larger than $(8/\pi)H_c$ in order to have domain in motion. The magnitude of ΔH_1 was defined in Equation 39. In the case of the applied field, $\bar{H}_{A-B}$ or $\bar{H}_{B-C}$, H_1 can be calculated according to Equation 67. Since most magnetic materials used for bubble device applications have small coercivity, H_c, it will be considered here that H_c is negligibly small and remains constant when domain is in motion. It also will be assumed here that the domain velocity is proportional to the driving field ΔH_1 with the proportional constant remaining the same and independent of the magnitude of the driving field. Although the diameter of domain will change during the propagation, the driving field defined in Equation 39 will be used according to the proper fixed domain diameter, such as initial diameter of circular domain. With these assumptions, it can be seen that the magnitude of domain velocity is proportional to H_1 or gradient of the applied field.

Domain motion in permalloy propagating circuit has been so far considered to be straight line propagation. The applied field produced by the permalloy bars has been calculated for variation of x only. Consequently, the direction of domain translation is along the direction of maximum velocity. Figures 12 and 13 show the negative of the first derivative of the applied field $\bar{H}_{A-B}$ and $\bar{H}_{B-C}$, respectively. Both figures show that the domain velocity is not constant and in fact, is increasing from the start to the finish. It should be noted that they

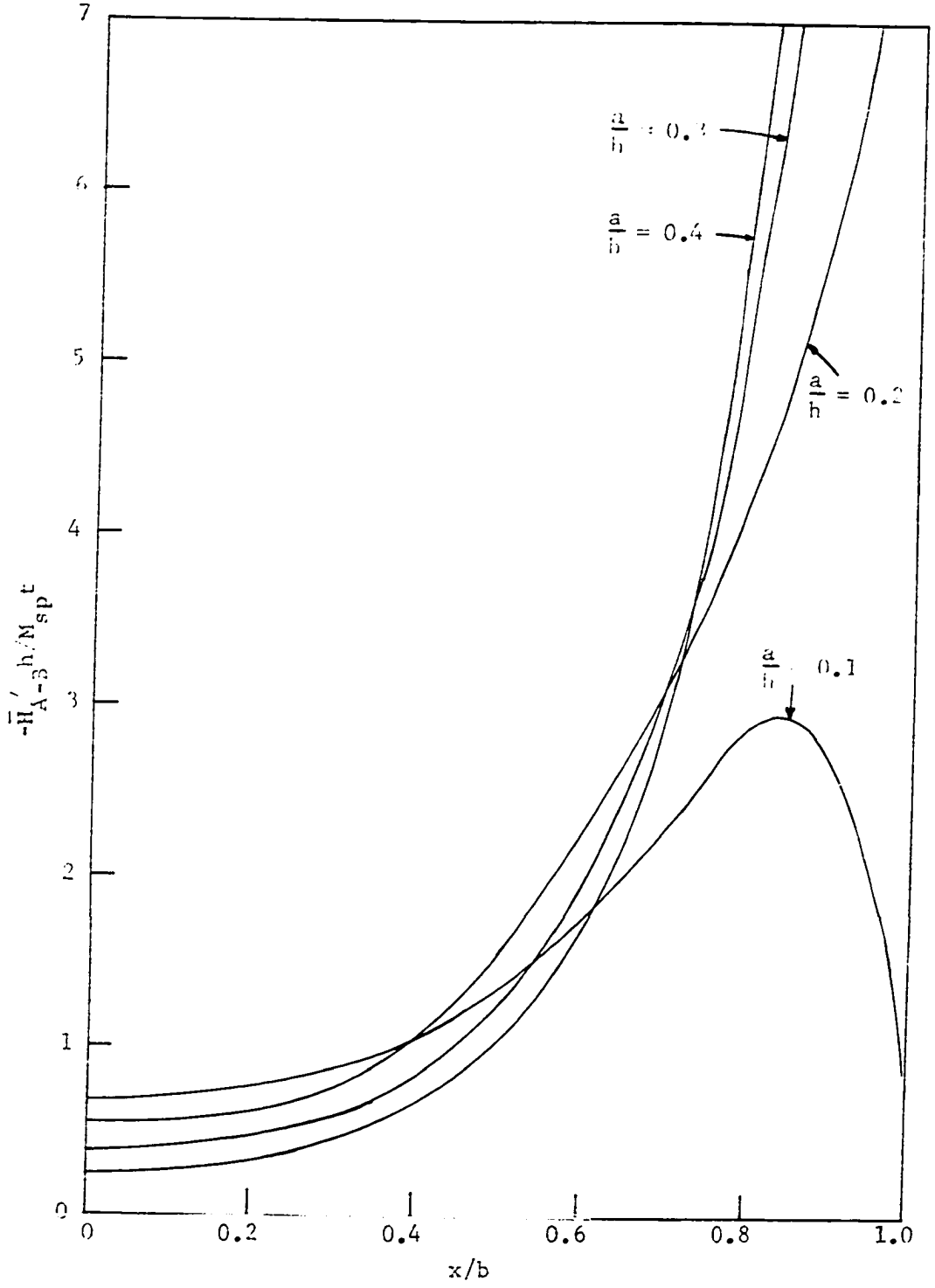

Figure 12. Variation of H_1 for $\bar{H}_{A-B}$ along the channel

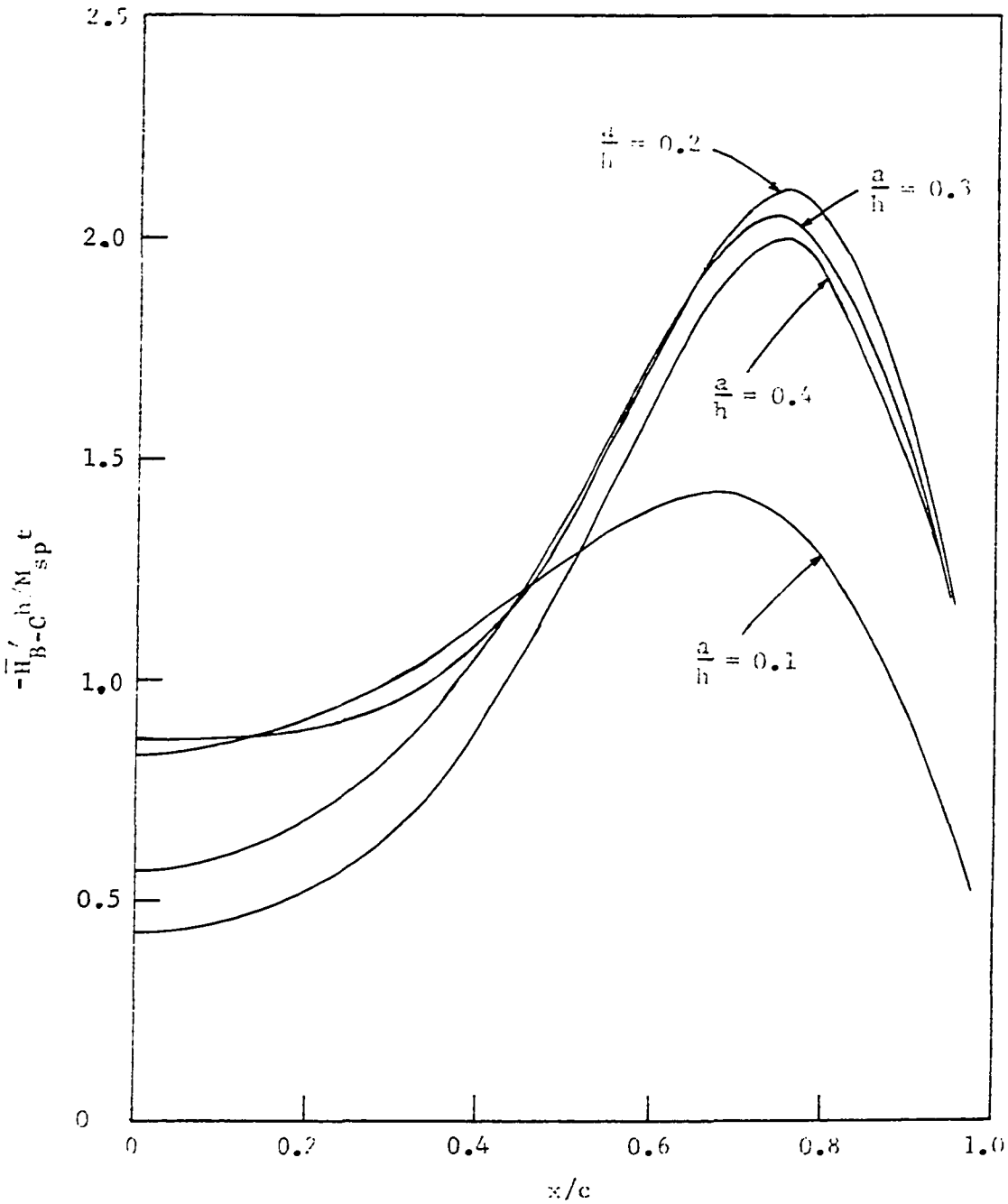

Figure 13. Variation of H_1 for $\bar{H}_{B-C}$ along the channel

have less significance at the ends as stated in the case of domain size change. It can be seen that the change of velocity is smaller at the start. The initial velocity is larger for smaller ratio of a to h in both cases. The initial velocity is important for domain pulling out of the stable positions produced by the isotropic permalloy which will be discussed in the next chapter. The velocity change is comparatively smaller for the narrow width of permalloy bars. It is desirable to have domain velocity as large and uniform as possible.

Change in domain shape, specifically elliptical change, can be determined by Equation 56. The shape-changing driving field, ΔH_2, has been defined in Equation 54. In Equation 56 domain coercivity acts as a dragging force to stabilize the domain shape variation. In the case of the applied field, $\bar{H}_{A-B}$ or $\bar{H}_{B-C}$, the driving field can be calculated by Equation 68. Consequently, the elliptical shape can be determined by examining the second derivative of the applied fields. Figures 14 and 15 show the negative of the second derivatives of $\bar{H}_{A-B}$ and $\bar{H}_{B-C}$ along the propagating channel. Both figures show that the elliptical variation is smaller at start of the domain translation. Variation of the width of the permalloy bars shows that domain shape change is smaller for narrow permalloy bars. In Figure 15 it also can be seen the possibility of exchanging the directions of major and minor semiaxes of the ellipse. Since most magnetic materials used for platelet have small domain coercivity in order to have high translating domain velocity, it is desirable to have driving field, ΔH_2, as small as possible. It

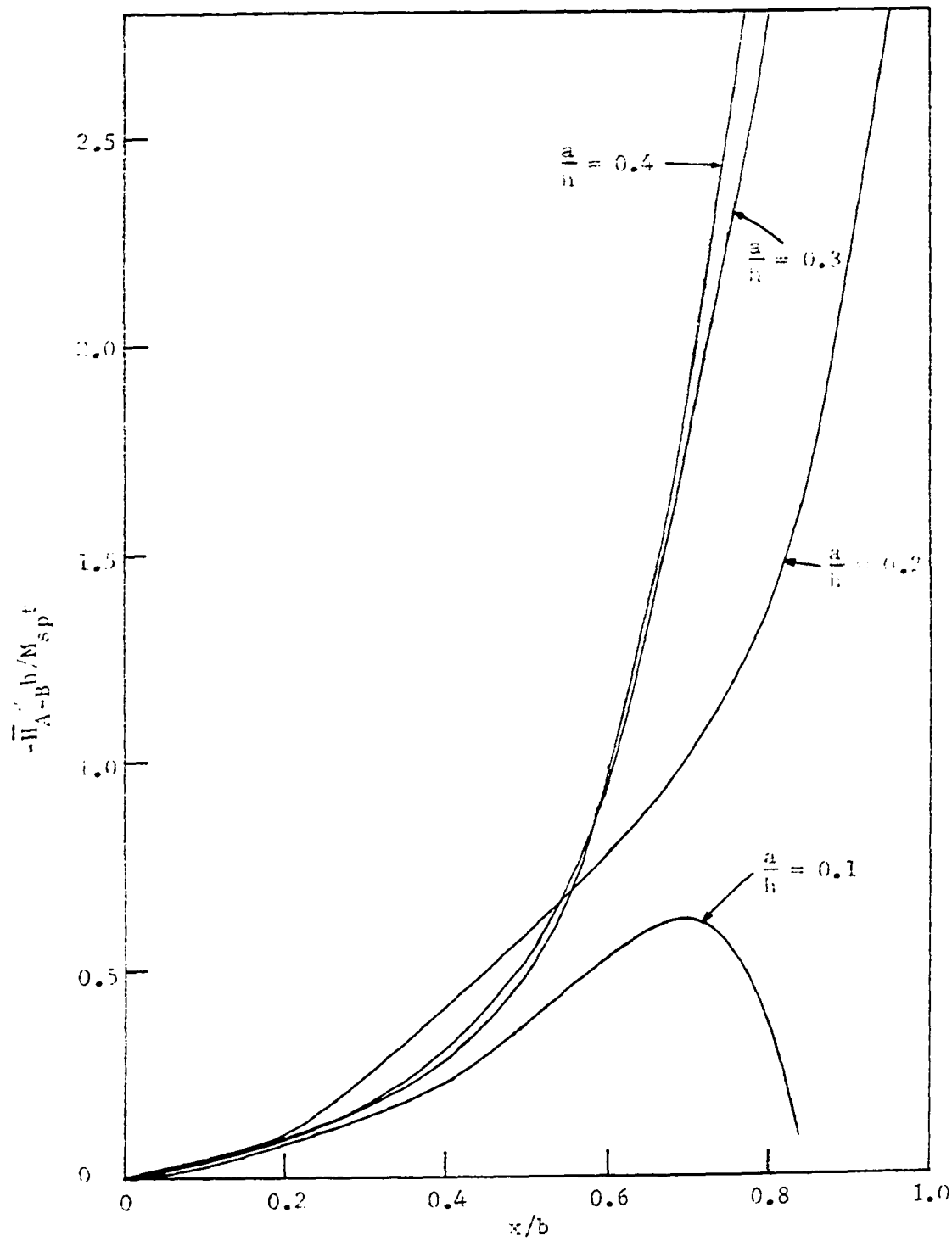

Figure 14. Variation of H_2 for $\bar{H}_{A-B}$ along the channel

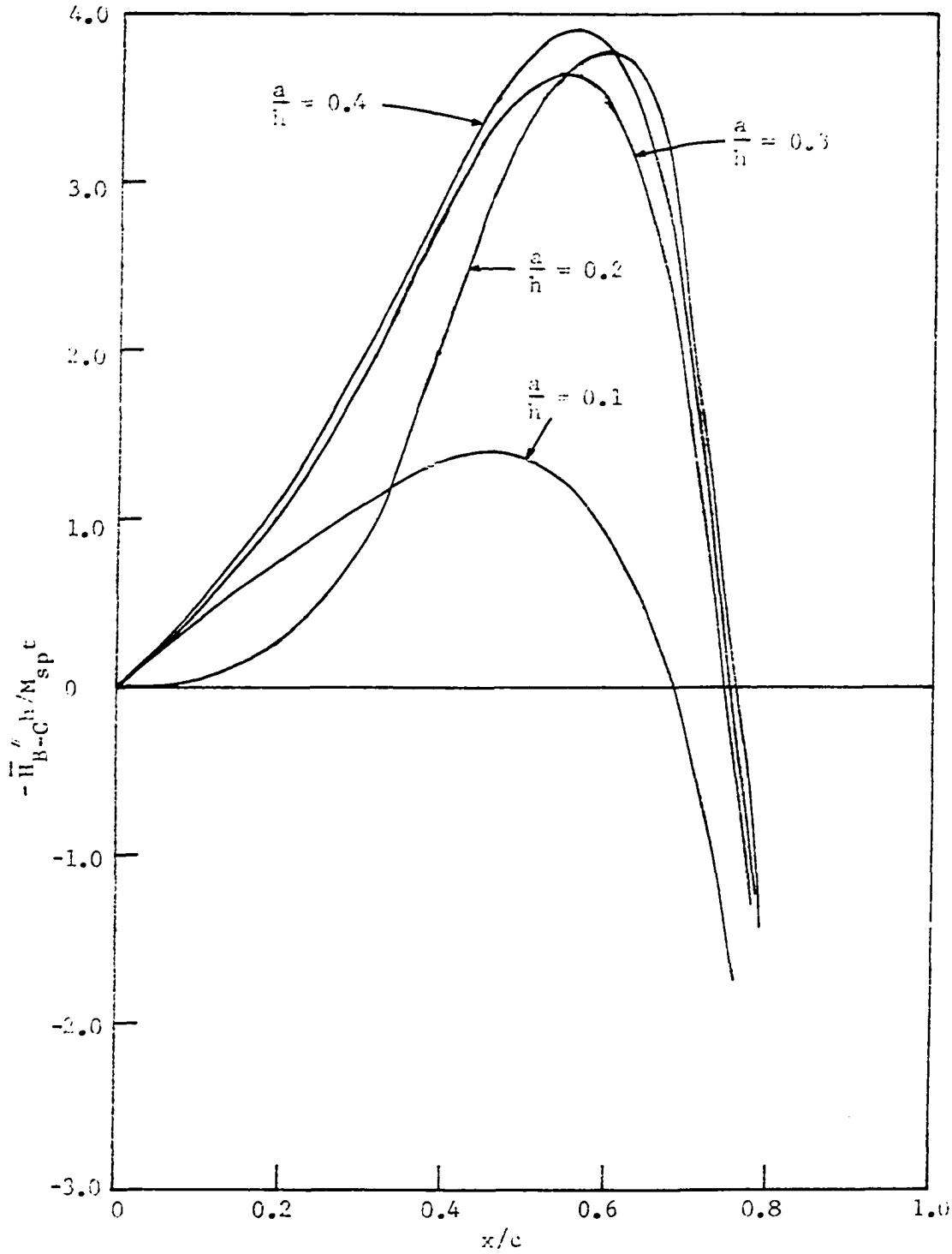

Figure 15. Variation of H_2 for $\bar{H}_{B-C}$ along the channel

should also be noted that if the applied field is biased at the elliptical run-out, the factor $1/[(\ell/h)-S_2(d/h)]$ in Equation 56 becomes infinite. Therefore, this factor should be taken into account in evaluation of domain shape variation.

3. Discussions

The magnetic cylindrical domains can be propagated by applying localized field gradient and permalloy propagating circuit provides the field gradient to move domains by applying transverse rotating magnetic field. The fields, however, produced by the magnetic poles at the ends of the permalloy bars do not provide uniform field gradient. At each step the field gradient changes slowly at the start of the domain translation and changes drastically when approaching to the end. Consequently, the velocity of domain propagation is not constant and it increases when a domain is approaching to the end of the permalloy bar. Simultaneously, change in domain size and shape is accompanying with domain motion. Experimentally, Rossol (10) has observed these phenomena using stroboscopic observation of domain motion in T-bar structure. It is desirable to have a circuit to provide uniform field gradient and to have this field gradient as large as possible within the range of stable bubble domain. For the permalloy-bar circuit, the initial velocity seems to be too small to operate at high frequency rate. If the elliptical change in domain shape is too large, it increases the detection difficulty and possibly gives the false information. Permalloy circuit does have this problem if the second order derivative of the applied field is too large.

It has been assumed that the domain wall energy is isotropic in the above analysis. Della Torre and Dimyan (39) have shown that anisotropy of wall energy exists in orthoferrites. This anisotropy of wall energy causes domains initially to be elliptical. Using energy variation expression, the ellipticity of domain resulted from this anisotropy can be calculated (see Appendix B). Therefore, evaluation of change in domain shape should include this effect in addition to the change due to nonuniform field gradient. Permalloy propagating circuit, however, does provide a simple and easy way to manipulate the bubble domain.

The effect on the variation of the applied field by the width of permalloy bars has been considered in the above analysis. Several values of the width have been compared. It showed that the wider permalloy bars have smaller change in domain size, but the narrower bars have more uniform velocity, higher initial velocity, and smaller deformation. Since the most important factor in practical applications is domain velocity, it is better to have narrow width of permalloy bars in the propagating circuit. Preparing the periodic thin permalloy film circuit, such as T-bars, is accomplished by the standard photolithographic techniques. It still has limitation of linewidth in the etching of permalloy films. Recently a technique based on electroless deposition has been developed (40). Therefore, a circuit of narrow linewidth is currently attainable. From circuitwise consideration permalloy propagating circuit is more suitable for bubble materials having small domain size in order to operate at high data rates. Garnets and hexagonal ferrites have smaller domain diameters than orthoferrites. However, the selection of materials for bubble devices

which operate at high data rates requires consideration of the domain-wall mobility as well as the domain diameter. For fixed drive field orthoferrites have highest domain-wall velocity. Comparison of data rates of these materials has been investigated by Bobeck (22).

The analysis of domain motion has been considered only for straight line propagation. The domain velocity defined in Equation 42 is the maximum velocity in the direction of maximum driving field. It was noted before that in general energy variation expression, Equation 27, there is a torque to turn a domain into the direction of maximum driving field. Thus, for a straight line propagation a domain moves with its maximum velocity. In the practical bubble devices, the bubble does not always propagate in a straight line. When the bubble changes its propagating direction, such as turning the corner, time is required to recover its maximum speed in the new direction. Consequently, the bubble may possibly be trapped at a corner position when the bubble devices are operating at high data rate. This could be one of the reasons which cause the failure of faster domain propagation at sharp angle turn.

A periodic permalloy propagating circuit, such as T-bar and Y-bar structures, has symmetric pattern which can be used to propagate the bubble in both directions. For the purpose of unidirection propagation the permalloy elements can be modified to have directionality using the fact that the permalloy elements serve as localized flux closure paths thereby reducing the magnetostatic energy. This may provide a speed advantage. The Y-bar structure has the advantage over T-bar structure for its having four about equal pole strength positions, but consideration

that in Y-bar circuit domain has to change its direction of propagation in a single period should be taken into account. Comparison of permalloy propagating circuit with current conductor circuit may show that current conductor circuit can provide more uniform field gradient and higher velocity at the expense of complexity of circuit preparation.

D. Analysis of Force Exerted by a Permalloy Bar on a Magnetic Domain

In the previous analysis of bubble domain motion, the effect of permalloy system on domain motion has not been considered. Without applying the transverse rotating field, there exists a magnetostatic interaction between bubble domains and permalloy films. A magnetic cylindrical domain prefers a position in contact with the permalloy, because the permalloy serves as localized flux closure paths thereby reducing the magnetostatic energy. In other words, there is a force exerted by a cylindrical domain on a permalloy film. This force will affect the domain motion in the permalloy propagating circuit.

Now consider the change in energy when a magnetic object of permeability μ_1 is placed in a magnetic field whose free magnetic pole sources are fixed. Initially the magnetic field $\vec{H}_o$ due to a certain distribution of free magnetic charges exists in a medium of permeability μ_o. The initial magnetostatic energy is (in Gaussian units)

$$W_o = \frac{1}{8\pi} \int \vec{H}_o \cdot \vec{B}_o \, d^3x \tag{69}$$

where $\vec{B}_o = \mu_o \vec{H}_o$. Then with the sources fixed in position an object of permeability μ_1 and volume V_1 is introduced into the field, changing the field from $\vec{H}_o$ to $\vec{H}$. The energy now has the value

$$W_1 = \frac{1}{8\pi} \int \vec{H} \cdot \vec{B} \, d^3x \tag{70}$$

where $\vec{B} = \mu_1 \vec{H}$. The difference in the energy can be written as

$$W = \frac{1}{8\pi} \int (\vec{H} \cdot \vec{B} - \vec{H}_o \cdot \vec{B}_o) d^3x$$

$$= \frac{1}{8\pi} \int (\vec{H} \cdot \vec{B}_o - \vec{B} \cdot \vec{H}_o) d^3x + \frac{1}{8\pi} \int (\vec{H} + \vec{H}_o) \cdot (\vec{B} - \vec{B}_o) d^3x \tag{71}$$

Since $\vec{\nabla} \times (\vec{H} + \vec{H}_o) = 0$ because of no current source, this implies

$$\vec{H} + \vec{H}_o = - \vec{\nabla} \phi_m \tag{72}$$

Thus the second integral of Equation 71 becomes

$$I = - \frac{1}{8\pi} \int \vec{\nabla} \phi_m \cdot (\vec{B} - \vec{B}_o) d^3x \tag{73}$$

Integration by parts yields

$$I = \frac{1}{8\pi} \int \phi_m \vec{\nabla} \cdot (\vec{B} - \vec{B}_o) d^3x = 0 \tag{74}$$

since $\vec{\nabla} \cdot (\vec{B} - \vec{B}_o) = 0$ because the source charge is assumed unaltered by the insertion of the permeable object. Consequently, the energy change is

$$W = \frac{1}{8\pi} \int (\vec{H} \cdot \vec{B}_o - \vec{B} \cdot \vec{H}_o) d^3x \tag{75}$$

Since outside V_1, $\vec{B} = \mu_o \vec{H}$, the integration will be only over the volume V_1 of the object. It becomes

$$W = -\frac{1}{8\pi}\int_{V_1}(\mu_1 - \mu_o)\vec{H}\cdot\vec{H}_o\, d^3x \tag{76}$$

If the medium surrounding the permeable body is free space, then $\mu_o = 1$. Using the definition of magnetization M, Equation 76 can be expressed as

$$W = -\frac{1}{2}\int_{V_1}\vec{M}\cdot\vec{H}_o\, d^3x \tag{77}$$

where $\vec{M}$ is the magnetization of the object.

Equations 76 and 77 show that a permeable body will tend to move towards regions of increasing H_o provided $\mu_1 > \mu_o$. There will be a change in the energy δW by imagining a small generalized displacement of the body δx. Since the magnetic charges are held fixed, there is no external source of energy and the change in field energy must be compensated for by a change in the mechanical energy of the body. This means that there is a force acting on the body

$$F_x = -\left(\frac{\partial W}{\partial x}\right) \tag{78}$$

In order to calculate the force exerted by a cylindrical domain or bubble on a permalloy film, the permalloy film will be assumed to be thin enough so that only the radial field produced by a bubble is effective for the magnetization induced in the permalloy. The radial bubble field is determined by considering to be the same as the field due to a thin cylindrical current sheet with the height of the bubble thickness. First the magnetic field from a circular current loop is calculated. This field then is integrated over the entire bubble

thickness. Converting the current source to the magnetization using the standard method yields the radial bubble field. Figure 16 shows the coordinate system used to calculate the radial field from a bubble. The domain is assumed to be circular with radius r_o. Appendix C shows that the radial component of the field from a current loop is (in Gaussian units)

$$H_\rho = \frac{I z k}{C \rho^{\frac{1}{2}} r_o^{\frac{1}{2}}} \left[\left(\frac{1 - \frac{k^2}{2}}{1 - k^2} \right) E(k) - K(k) \right] \tag{79}$$

where I is the current, z is the distance above the plane of the loop at which the field is calculated, ρ is the radial distance, K and E are the complete elliptic integrals of the first and second kind, respectively, and k is the modulus of the elliptic integrals. Integrating over the entire bubble thickness h and then converting the current to the magnetization yield the radial bubble field which is given by (Appendix C)

$$H_\rho = 4M_{sd} \left(\frac{r_o}{\rho}\right)^{\frac{1}{2}} \left\{ \left[2 \left(\frac{K(k_1) - E(k_1)}{k_1} \right) - k_1 K(k_1) \right] \right.$$

$$\left. - \left[2 \left(\frac{K(k_2) - E(k_2)}{k_2} \right) - k_2 K(k_2) \right] \right\} \tag{80}$$

where M_{sd} is the magnetization of the bubble,

$$K_1^2 = \frac{4 r_o \rho}{z^2 + (r_o + \rho)^2} \tag{81}$$

and

$$k_2^2 = \frac{4 r_o \rho}{(z+h)^2 + (r_o + \rho)^2} \tag{82}$$

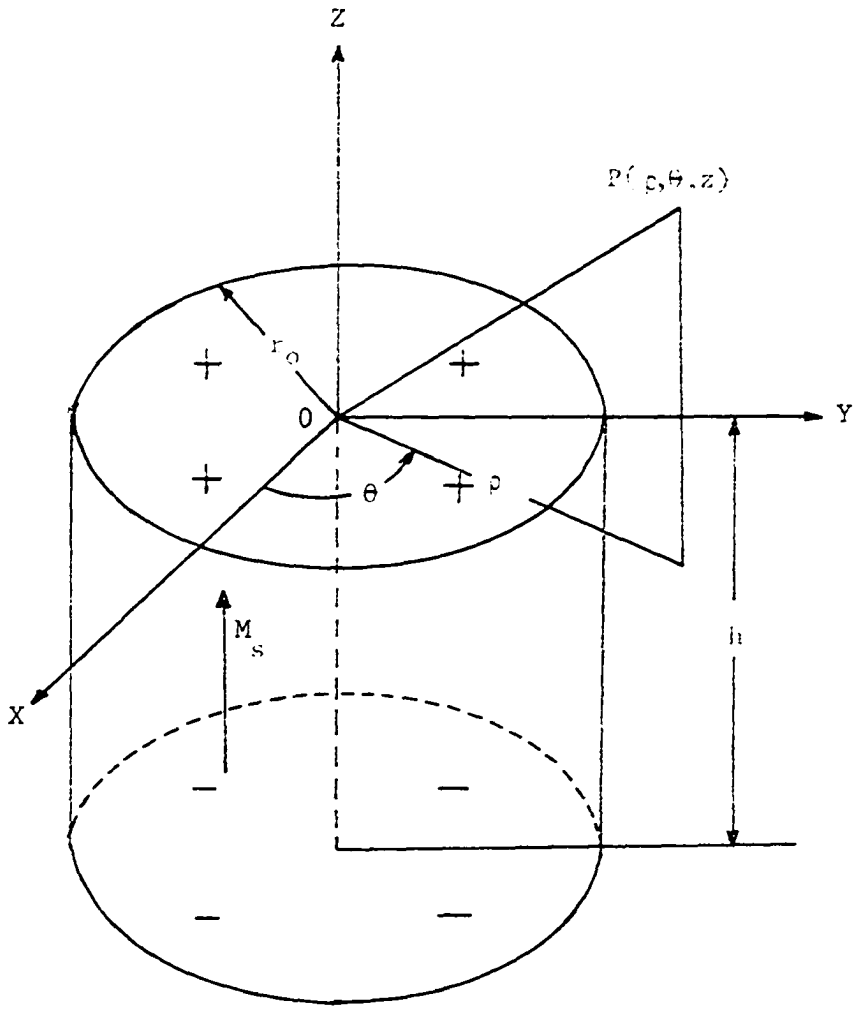

Figure 16. Coordinate system for calculating the radial field from a bubble

Snow (41) has calculated the magnetic field from a thin cylindrical current sheet using different approach. Similar result of Equation 80 also has been obtained by the others (27). Figure 17 shows the radial field from a bubble for three different radii of domains for the case $z = 0.1h$. As can be seen in the figure, the radial field is strongest at the vincinity of the domain wall.

In order to calculate the force using Equation 78, the magnetization induced in the permalloy by the radial bubble field has to be determined. Since permalloy is a ferromagnetic material, there is a nonlinear functional relationship between the magnetization M and the applied field H. This phenomenon of hysteresis implies that M is not a single-valued function of H. This complicates the problem to determine the magnetization of permalloy. If the radial bubble field is much larger than the coercivity and demagnetizing field induced by the bubble field, the magnetization of the permolloy film will be saturated. The idealized hysteresis loop of permalloy is almost rectangular and the coercivity is usually very small so that a linearized and single-valued M-H curve will be used to approximate the magnitude of the magnetization when the bubble field is smaller than the demagnetizing field. The equations for the demagnetizing factors of a planar film can be computed from formulae given by Osborn (42) for a general ellipsoid. Approximating the thin film permalloy with dimension length (ℓ) × width (w) × thickness (t) of a flat ellipsoid (43), the demagnetizing factors for $\ell > w \gg t$ are

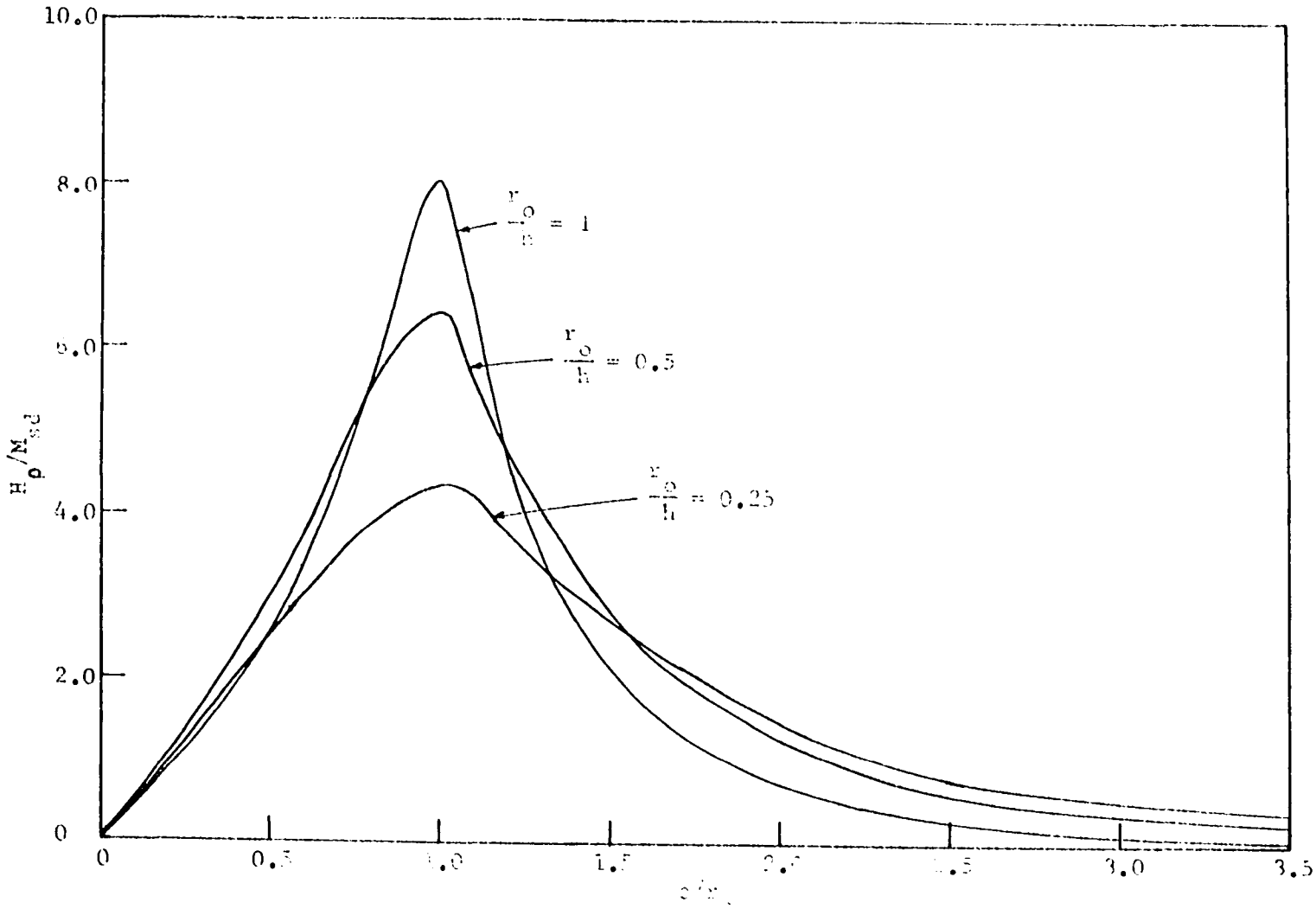

Figure 17. Radial bubble fields for three different ratios of $\frac{r_o}{h}$

$$N_{\ell} = (\frac{t}{\ell})(1 - e^2)^{\frac{1}{2}}(\frac{K(k) - E(k)}{e^2}) \tag{83}$$

$$N_w = (\frac{t}{\ell}) \frac{E(k) - (1 - e^2)K(k)}{e^2(1 - e^2)^{\frac{1}{2}}} \tag{84}$$

where

$$e^2 = 1 - (\frac{w}{\ell})^2 \tag{85}$$

and K and E are the complete elliptic integrals of the first and second kind, respectively, and $k = [1-(w/\ell)^2]^{\frac{1}{2}}/[1-(t/\ell)^2]^{\frac{1}{2}}$ is the modulus. As stated before, t is small enough so that the magnetization is in the plane of the film and N_t need not be considered.

Figure 18 shows the demagnetizing factors of N_{ℓ} and N_w as a function of film thickness. It shows that the demagnetizing factors are almost proportionally increasing with thickness of the film. As the film thickness gets larger, the formulae can not be applied any more. The corresponding demagnetizing fields along the film length and width are given, respectively, by

$$H_{D\ell} = - 4\pi N_{\ell} M_{sp} \tag{86}$$

and

$$H_{Dw} = - 4\pi N_w M_{sp} \tag{87}$$

where M_{sp} is the saturated magnetization of permalloy. Now suppose that $4\pi M_{sd}$ of the bubble material is 100 Gauss and $4\pi M_{sp}$ of permalloy is 10^4 Gauss. Comparison of the radial bubble field (Figure 17) with the demagnetizing field of permalloy film (Figure 18) shows that permalloy film can only be saturated at the vicinity of domain wall

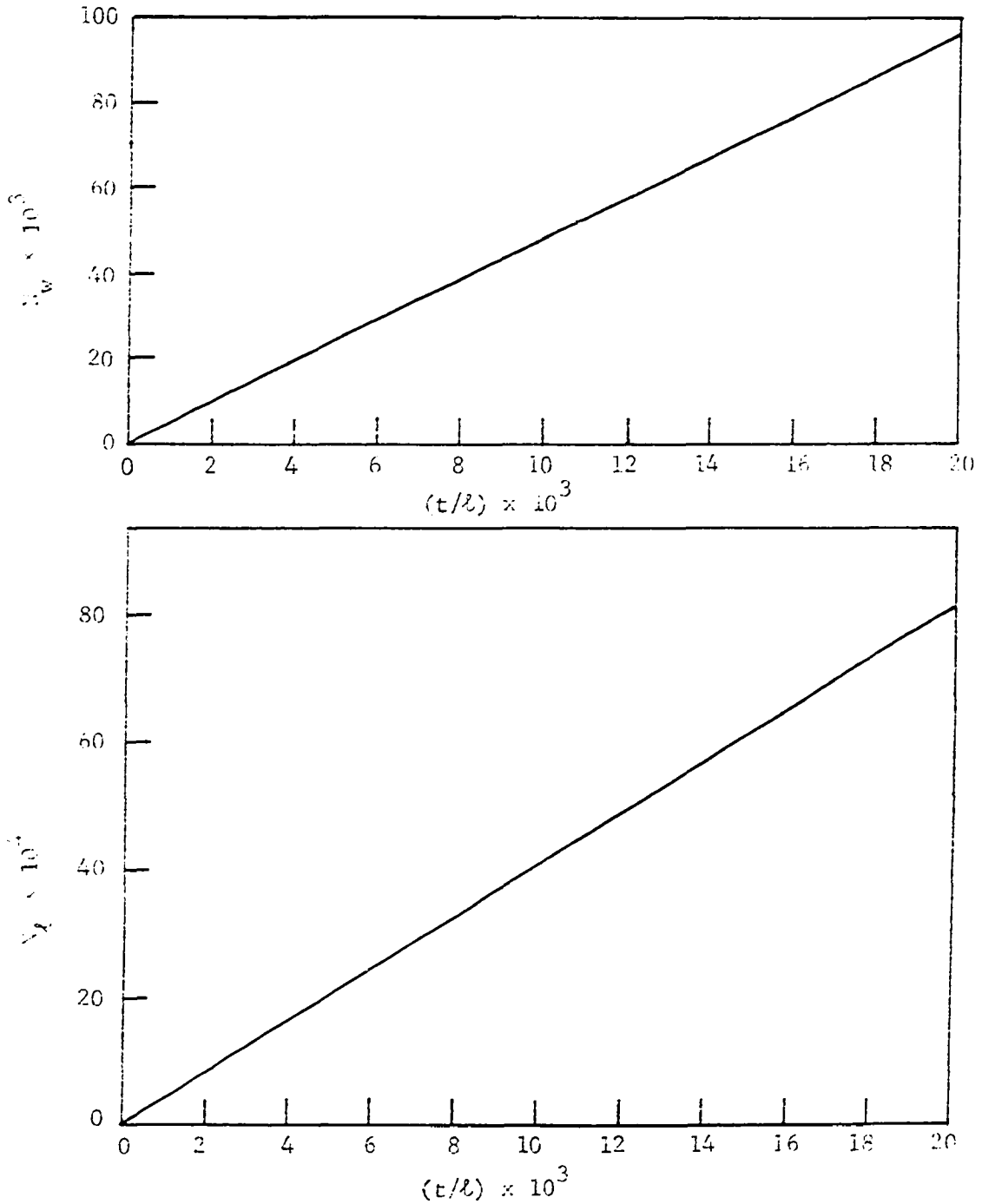

Figure 18. Demagnetizing factors, N_ℓ and N_w, as a function of film thickness

when the bubble is across the film length. Consequently, the approximation using linearized M-H curve will be used to determine the magnetization.

Substituting the calculated radial bubble field, Equation 80, and the approximate magnetization into Equation 78 yields the force exerted by a bubble on a permalloy film. Two cases of the force, bubble across the film length and width, will be computed. These forces are given by

$$F_{\ell}(x) = \frac{1}{2}\int_{-a}^{a} t_p M(x',y) H_{\rho}(x',y)\Big|_{x'=x-b}^{x'=x+b} dy \tag{88}$$

and

$$F_{w}(x) = \frac{1}{2}\int_{-b}^{b} t_p M(x',y) H_{\rho}(x',y)\Big|_{x'=x-a}^{x'=x+a} dy \tag{89}$$

where x is the distance between the centers of the bubble and the permalloy film, and the film dimension is length (2b) × width (2a) × thickness (t_p). Numerical calculation of Equations 88 and 89 can then be performed. Figures 19 and 20 show plots of F_{ℓ} and F_{w}, respectively, exerted by a permalloy film of $a/r_o = 0.7$. Two cases of different bubble radii, $r_o/h = 0.5$ and $r_o/h = 0.25$, are also shown in these figures.

It is clear from Figure 19 that a bubble initially at the outside of permalloy film and across the length of film would experience an attractive force pulling it towards the permalloy. This attractive force will reach maximum just after the leading edge of the bubble domain passes one end of permalloy film. It decreases till the point where the center of the bubble right at the end edge of permalloy and then increases again to the other peak, which is a little less than the

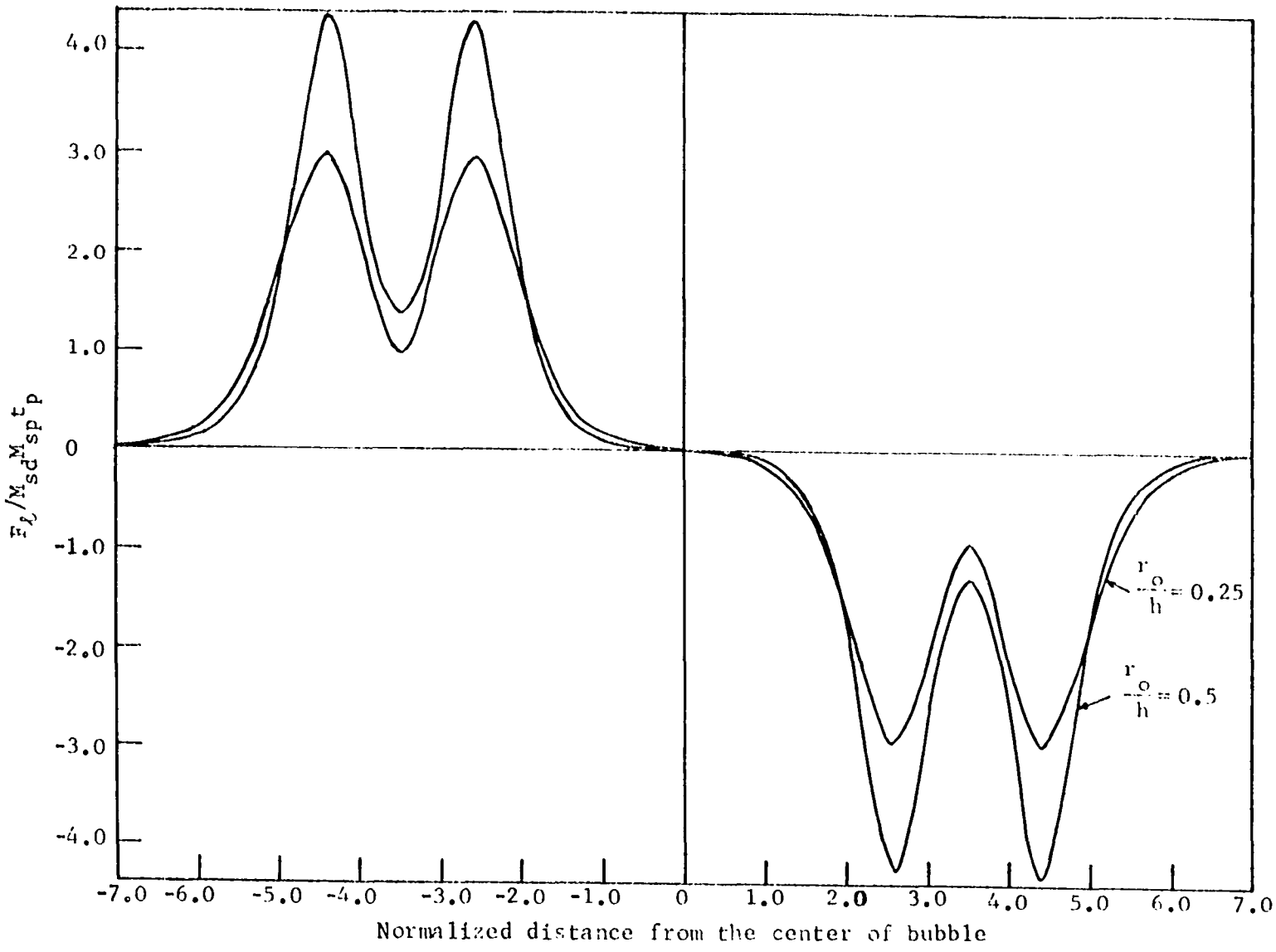

Figure 19. Force exerted by a permalloy on bubble across film width

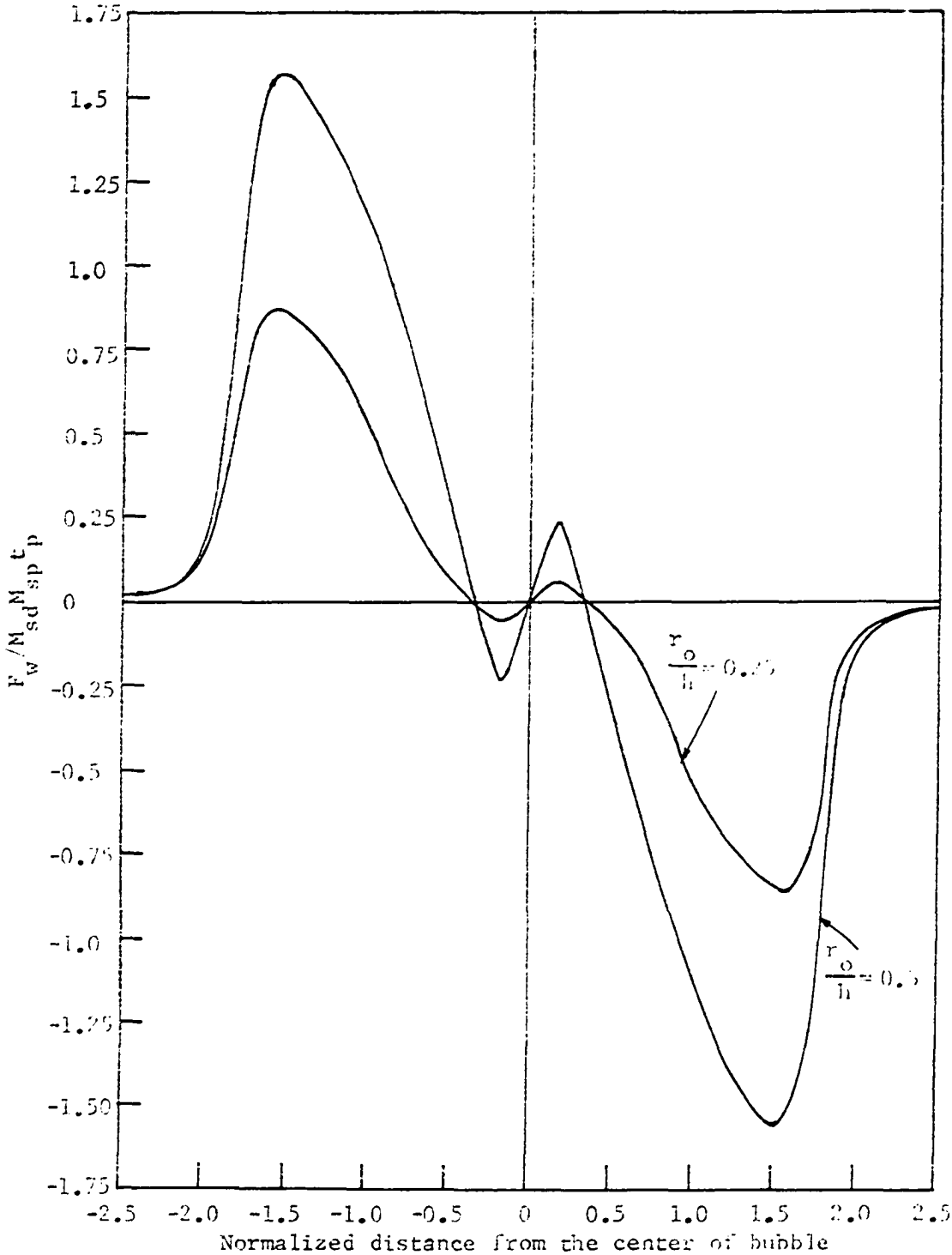

Figure 20. Force exerted by a permalloy on bubble across film width

maximum, when the trailing edge of the bubble domain just before passes the end of permalloy. The attractive force goes to zero when the centers of the bubble and the film coincide. Whether or not the bubble reaches the center of film is dependent on the coercivity of the material which for the discussion of this figure shall be assumed negligible. Once the bubble at the center of permalloy film, an external force is required to move the bubble out from the permalloy film. Consequently, when a bubble is propagating in a permalloy circuit, an extra force is required to pull the domain out of lower magnetostatic energy position due to the effect of the interaction between bubble and permalloy. In a T-bar propagating circuit such as shown in Figure 7, it can be seen from Figure 19 that the force required to move a bubble out from position A to B is rather small without considering the effect of the vertical bar of the T. This force, however, is required much larger to move the bubble out from position B to C. Therefore, the initial driving field for each step of domain propagation in the permalloy circuit has to be large enough to overcome the force exerted on the bubble by the permalloy in addition to the coercivity of the bubble. This becomes more important when the bubble device is operating at higher data rates. The improved Y-bar arrangement of permalloy propagating circuit having a well-localized pole over T-bar provides higher driving field for moving bubble out of position B, so that it may possibly operate at higher data rates than T-bar arrangement.

For the case of a bubble moving across the width of a permalloy bar, Figure 20 shows that the same attractive force exists to pull the

bubble towards the permalloy bar. The magnitude of this force is smaller than the first case due to higher demagnetizing factor across the width of the permalloy film. The force has only one peak instead of two at the point where the leading edge of bubble domain just passes the edge of permalloy film. A large amount of external force is also required to pull bubble completely off the permalloy. This implies that the applied driving field in permalloy propagating circuit (from position C to D in Figure 7) should be larger than this pull-off in order to have bubble propagation. It is interesting to note that in Figure 20 there exists two stable positions of the bubble with respect to the permalloy film, one at each side of the center. It can be seen in the figure that an external force is required to move bubble from one stable position to the other. This bistable condition for bubbles can be used to provide permalloy rail coupled channel system (44) by optimizing the width of the permalloy film.

For the purpose of bubble propagation at high data rates, it is desirable to have the pull-off force as small as possible so that the applied field is at the least expense of energy. It can be seen from Figures 19 and 20 that the maximum pull-off force is smaller for smaller domain radius because the radial bubble field is smaller as shown in Figure 17. The nominal radius of bubbles commonly used in permalloy propagating circuit is around $r_o/h = 0.3$ (9, 38), instead of the preferred value given by Thiele (7). Equations 88 and 89 shows that decreasing the magnetization might decrease the pull-off force. For very thin film the demagnetizing factor is approximately proportional

to the thickness of permalloy film as shown in Figure 18. Increasing the thickness may provide less magnetization but the force is also proportional to the thickness so that increasing thickness does not help to decrease the pull-off force. It, however, provides stronger pole strength at the ends of permalloy bars and accordingly produces larger driving field. It is clear that the maximum of the pull-off force occurs at the time when a bubble is about completely off the permalloy. Consequently, a rather large initial driving field is required at each step, such as from B to C in Figure 7. This gives the advantage for current-conductor drive circuit because of the limitation of all permalloy circuit yielded by its circuit configuration and natural property. After a bubble moves out a permalloy bar and when it approaches to the other one, the magnetostatic interaction acting as an attractive force forces the bubble towards the permalloy. This alsc results in the increase of bubble propagating speed in addition to the increase produced by the applied nonuniform gradient field.

Since the domain wall of bubbles is assumed to be cylindrical, the domain has reflection symmetry through the central plane of the platelet. It is possible to use permalloy circuit at both sides, top and bottom, of the platelet to propagate cylindrical magnetic domains. The circuit pattern of permalloy for both sides may be designed to be complement to each other. Thus, the bubble will ride at least above or underneath the permalloy all the time in propagation. The force induced by the magnetostatic interaction is considerably small when the bubble stays above or underneath the permalloy compared to the force required to pull it

completely off the permalloy. Consequently, using both sides of the platelet for permalloy propagating circuit may provide speed advantage. Moreover, it possibly doubles the strength of applied driving field.

IV. SUMMARY AND CONCLUSIONS

Theroetical study of dynamic behavior of cylindrical magnetic domains, specifically propagating in the permalloy circuit, has been established in this research. The main results of the study are summarized as follows:

1. A cylindrical magnetic domain will experience a force attempting to move it towards a position of reduced bias when a localized field gradient is applied. If the applied gradient is nonuniform, the response could involve motion at a nonuniform rate and change in size and shape. Using Fourier decomposition of the applied field and considering in the presence of dissipative processes, the results show that the constant term of the applied field determines domain size, the θ term translates the domain, and the $n\theta$ terms, for $n \geq 2$, deform the domain. The domain velocity expression, Equation 42, has the same form as the case of uniform field gradient, but the driving field varies at each point of propagating circuit so that domain motion is at highly nonuniform rate. Calculation of the magnetic fields from practical permalloy propagating circuit shows that the applied localized field is never uniform. Consequently, the domain velocity is nonuniform accompanying with changes in domain size and shape which was confirmed by the experimental observation (10).

2. Since the permalloy propagating circuit is currently seen as most attractive for device applications, calculation of magnetic field produced by magnetized permalloy bars has been made. The variation of the calculated fields for two types of discrete step of domain propagation

shows generally that initial driving field is much smaller than the field at the rest of the time. Due to the magnetostatic interaction between magnetic domain and highly permeable permalloy films, there exists a force exerted on the bubble by the permalloy bar. Calculation of the force shows that a large amount of external force is needed to pull the bubble completely off the permalloy. The starting position of the bubble for most propagating steps in the permalloy circuit is at the end of the permalloy bar (see Figure 7) so that an extra initial force is needed to overcome the pull-off force in order to propagate the bubble. In device applications, operation at high data rates is desirable. Therefore, the propagating circuit is preferable to have large initial driving field. Study of the effect on the magnetic field by the variation of the width of the permalloy bars shows that the narrower ones have larger initial driving field. Consequently, from circuit-wise consideration, permalloy propagating circuit is more suitable for smaller bubble domain size in order to operate at high frequency rate.

3. In this study coercivity has been assumed to be uniform and independent of the direction of wall motion. Under this assumption a domain propagates in the direction in which the domain velocity is maximum, i.e., the direction in which the bias field decreases most rapidly. Therefore, for a straight line propagation, a domain translates with its maximum speed. This can be seen in general energy variation expression that there exists a torque to turn the domain into this direction. When the domain changes its propagation direction, such as turning a corner, time is required to recover its maximum speed in the

new direction. Moreover, at the step to turn the corner in the permalloy propagating circuit only the magnetized pole at one side of the domain provides the local magnetic field gradient. The driving field, and thereby the velocity, are smaller than at the rest of the steps. Consequently, operating at higher frequencies, the domain propagation fails, and the domain becomes trapped at a corner position. The design of the corner is thus the first obstacle to faster domain propagation in the permalloy propagating circuit.

4. For the purpose of faster domain propagation, it is undesirable to have magnetostatic interaction between the bubble and the permalloy film, especially at the start of each propagating step. Calculation of pull-off force shows that decreasing the ratio of the domain radius to the thickness decreases the pull-off force (Figure 19 and Figure 20). This magnetostatic interaction force is unavoidable in the permalloy circuit, but the force is considerably smaller when the bubble stays in contact with the permalloy compared to the force required to pull it completely off the permalloy. Since the domain has reflection symmetry through the central plane of the platelet, it is possible to use both sides of the platelet for permalloy propagating circuit. If the circuit pattern at both sides is designed to be complement to each other, the bubble would ride at least one side of the permalloy all the time in propagation. This may help to decrease the power wasted in cancelling the pull-off force and thereby to increase the domain speed. It also approximately doubles the driving field. Study of this magnetostatic

interaction is useful in designing permalloy rail coupled-channel system (44) and the calculated radial bubble field, Equation 80, also helps in designing the magnetostatic detector for bubble domains (45).

V. LITERATURE CITED

1. Broadbent, K. D. A thin magnetic film shift register. IRE Trans. Electronic Computers Ec-9: 321-323. 1960.

2. Spain, R. J. Controlled domain tip propagation. Part I. J. Appl. Phys. 37: 2572-2583. 1966.

3. Spain, R. J. and Jauvtis, H. J. Controlled domain tip propagation. Part II. J. Appl. Phys. 37: 2584-2593. 1966.

4. Michaelis, P. C. A new method of propagating domains in thin ferromagnetic films. J. Appl. Phys. 39: 1224-1226. 1968.

5. Bobeck, A. H. Properties and device applications of magnetic domains in orthoferrites. Bell Syst. Tech. J. 46: 1901-1925. 1967.

6. Bobeck, A. H., Fischer, R. F., Perneski, A. J., Remeika, J. P., and Van Uitert, L. G. Application of orthoferrities to domain-wall devices. IEEE Trans. Magnetics MAG-5: 544-553. 1969.

7. Thiele, A. A. The theory of cylindrical magnetic domains. Bell Syst. Tech. J. 48: 3287-3335. 1969.

8. Thiele, A. A. Theory of the static stability of cylindrical domains in uniaxial platelets. J. Appl. Phys. 41: 1139-1145. 1970.

9. Perneski, A. J. Propagation of cylindrical magnetic domains in orthoferrites. IEEE Trans. Magnetics MAG-5: 554-557. 1969.

10. Rossol, F. C. Stroboscopic observation of cylindrical domain propagation in a T-bar structure. IEEE Trans. Magnetics MAG-6: 500-501. 1970.

11. Kooy, C. and Enz, U. Experimental and theoretical study of the domain configuration in the layers of $BaFe_{12}O_{19}$. Phil. Res. Repts. 15: 7-29. 1960.

12. Gianola, U. F., Smith, D. H., Thiele, A. A., and Van Uitert, L. G. Material requirements for circular magnetic domain devices. IEEE Trans. Magnetics MAG-5: 558-561. 1969.

13. Chikazumi, S. Physics of magnetism. New York, N.Y., John Wiley and Sons, Inc. 1964.

14. Gyorgy, E. M. and Hagedorn, F. B. Analysis of domain-wall motion in canted antiferromagnets. J. Appl. Phys. 39: 88-90. 1968.

15. Van Uitert, L. G., Sherwood, R. C., Bonner, W. A., Grodkiewiez, W. H., Pictroski, L., and Zydzik, G. J. Rare earth orthoferrites for bubble domain devices. Mat. Res. Bull. 5: 153-161. 1970.

16. Van Uitert, L. G., Smith, D. H., Bonner, W. A., Gradkiewiez, W. H., and Zydzik, G. J. Hexagonal ferrites for bubble domain devices. Mat. Res. Bull. 5: 455-463. 1970.

17. Mee, C. D. The magnetization mechanism in single-crystal garnet slabs near the compensation temperature. IBM J. Res. Develop. 11: 468-476. 1967.

18. Nemchik, J. M. Circular domain configuration in GdIG. J. Appl. Phys. 40: 1086-1087. 1969.

19. Van Uitert, L. G., Bonner, W. A., Gradkiewiez, W. H., Pictroski, L., and Zydzik, G. J. Garnets for bubble domain devices. Mat. Res. Bull. 5: 825-835. 1970.

20. Bobeck, A. H., Spencer, E. G., Van Uitert, L. G., Abrahams, S. C., Barns, R. L., Grodkiewiez, W. H., Sherwood, R. C., Schmidt, P. H., Smith, D. H., and Walters, E. M. Uniaxial magnetic garnets for domain wall "bubble" devices. Appl. Phys. Lett. 17: 131-134. 1970.

21. Mee, J. E., Pulliam, G. R., Heinz, D. M., Owens, J. M., and Besser, P. J. Mobile cylindrical domains in epitaxial GA: YIG films. Appl. Phys. Lett. 18: 60-62. 1971.

22. Bobeck, A. H. A second look at magnetic bubbles. IEEE Trans. Magnetics MAG-6: 445-446. 1970.

23. Heinz, D. M., Besser, P. J., Owens, J. M., Mee, J. E., and Pulliam, G. R. Mobile cylindrical magnetic domains in epitaxial garnet films. J. Appl. Phys. 42: 1243-1251. 1971.

24. Rossol, F. C. Temperature dependence of rare-earth orthoferrites properties relevant to propagating domain device applications. IEEE Trans. Magnetics MAG-5: 562-565. 1969.

25. Rossol, F. C. Domain-wall mobility in rare-earth orthoferrites by direct stroboscopic observation of moving domain walls. J. Appl. Phys. 40: 1082-1083. 1969.

26. Seitchik, J. A., Doyle, W. D., and Goldberg, C. K. Simple method of measuring mobility in cylindrical domain materials. J. Appl. Phys. 42: 1272-1273. 1971.

27. Roosol, F. C. and Thiele, A. A. Domain wall dynamics using cylindrical domains. J. Appl. Phys. 41: 1163-1164. 1970.

28. Copeland, J. A. and Spiwak. R. R. Circular domain velocity versus force. Presented at the Intermag. Conf., Denver, Colo., 1971.

29. Rossol, F. C. Domain-wall mobility in Yttrium orthoferrite. Phys. Rev. Lett. 24: 1021-1023. 1970.

30. Thiele, A. A. Device implications of the theory of cylindrical magnetic domains. Bell Syst. Tech. J. 50: 725-773. 1971.

31. Thiele, A. A., Bobeck, A. H., Della Torre, E., and Gianola, U. F. The energy and general translation force of cylindrical magnetic domains. Bell Syst. Tech. J. 50: 711-724. 1971.

32. Galt, J. K. Motion of a ferromagnetic domain wall in Fe_3O_4. Phys. Rev. 85: 664-669. 1952.

33. Dillon, J. F., Jr. and Earl, H. E., Jr. Domain wall motion and ferromagnetic resonance in a maganese ferrite. J. Appl. Phys. 30: 202-213. 1959.

34. Asti, G., Colombo, M., Giudici, M., and Levialdi, A. Domain wall motion in Barium ferrite single crystals. J. Appl. Phys. 38: 2195-2198. 1967.

35. Callen, H. and Josephs, R. M. Dynamics of magnetic bubble domains with an application to wall mobility. J. Appl. Phys. 42: 1977-1982. 1971.

36. Copeland, J. A., Elward, J. P., Johnson, W. A., and Ruch, J. G. Single-conductor magnetic-bubble propagation circuits. J. Appl. Phys. 42: 1266-1267. 1971.

37. More, G. E., Jr. High-speed stroboscopic analysis of a current drive, magnetic domain propagation circuit. Presented at the Intermag. Conf., Denver, Colo., 1971.

38. Danylchuk, I. Operational characteristics of 10^3-bit garnet Y-bar shift register. J. Appl. Phys. 42: 1358-1359. 1971.

39. Della Torre, E. and Dimyan, M. Y. Anisotropy of wall energy in orthoferrites. IEEE Trans. Magnetics MAG-6: 489-492. 1970.

40. Reekstin, J. P. Fabrication of "bubble"-propagation circuit by electroless deposition of nickel-cobalt-phosphorous. J. Appl. Phys. 42: 1362-1363. 1971.

41. Snow, C. Magnetic fields of cylindrical coils and annular coils. National Bureau of Standards Appl. Math. Series 38. 1953.

42. Osborn, J. A. Demagnetizing factors of the general ellipsoid. Phys. Rev. 67: 351-357. 1945.

43. Coren, R. L. Shape demagnetizing effects in permalloy films. J. Appl. Phys. 37: 230-233. 1966.

44. Goldstein, R. M. and Copeland, J. A. Permalloy rail-cylindrical magnetic domain systems. J. Appl. Phys. 42: 2361-2367. 1971.

45. Almasi, G. S., Keefe, G. E., Lin, Y. S., and Thompson, D. A. Magnetoresistive detector for bubble domains. J. Appl. Phys. 42: 1268-1269. 1971.

46. Della Torre, E. Pressures on cylindrical magnetic domain walls. IEEE Trans. Magnetics MAG-6: 822-827. 1970.

47. Jahnke, E., and Ende, F. Tables of functions with formulae curves. 4th ed. New York, N.Y., Dover Publications, Inc. 1945.

VI. ACKNOWLEDGMENTS

The author wishes to express his deepest appreciation to his major professor, Dr. A. V. Pohm, for his constant guidance and many valuable discussions throughout this study.

A special word of thanks is expressed to the National Science Foundation for the financial support of the study.

VII. APPENDIX A

Evaluation of the first and second partial derivatives of the applied field interaction energy will be treated here. There are three terms, E_H^0, E_H^1, and E_H^2, in the energy expression, Equation 20. Since the same procedures can be applied to calculate the partial derivatives with respect to Δr_n and $\Delta\theta_n$ for all three terms, only evaluation of E_H^1 will be illustrated in the following.

Noting

$$\frac{\partial r_b(\theta)}{\partial r_n} = \cos n\,(\theta - \theta_n) \tag{A-1}$$

and

$$\frac{\partial r_b(\theta)}{\partial \theta_n} = n\Delta r_n \sin n\,(\theta - \theta_n) \tag{A-2}$$

and differentiating E_H^1 yield

$$\frac{\partial E_H^1}{\partial r_n} = 2hM_s H_1 \int_0^{2\pi} r_b^2(\theta) \cos n(\theta - \theta_n)\cos\theta\, d\theta \tag{A-3}$$

$$\frac{\partial E_H^1}{\partial \theta_n} = 2hM_s H_1 \int_0^{2\pi} r_b^2(\theta)\, n\Delta r_n \sin n(\theta - \theta_n)\cos\theta\, d\theta \tag{A-4}$$

$$\frac{\partial^2 E_H^1}{\partial r_n \partial r_m} = 4hM_s H_1 \int_0^{2\pi} r_b^2(\theta)\cos m\,(\theta - \theta_m)\cos n\,(\theta - \theta_n)\cos\theta\, d\theta \tag{A-5}$$

$$\frac{\partial^2 E_H^1}{\partial \theta_n \partial \theta_m} = 2hM_s H_1 \int_0^{2\pi} \{2r_b(\theta)\Delta r_n \Delta r_m\, n\, m \sin n(\theta - \theta_n)\sin m\,(\theta - \theta_m)$$

$$- r_b^2(\theta)\Delta r_n \delta_{mn}\, n\, m \cos m(\theta - \theta_m)\}\cos\theta\, d\theta \tag{A-6}$$

$$\frac{\partial^2 E_H^1}{\partial r_n \partial \theta_m} = 2\pi M_s H_1 \int_0^{2\pi} \{2r_b(\theta)\Delta r_m m \sin m(\theta - \theta_m) \cos n(\theta - \theta_n) + r_b^2(\theta)\delta_{mn} n \sin n(\theta - \theta_n)\} \cos\theta \, d\theta \tag{A-7}$$

where δ_{mn} is the Kronecker delta function. To evaluate these integrals, it is convenient to transform the integrands by using the trigonometric identities,

$$\sin x \cos y = \frac{1}{2}[\sin(x+y) + \sin(x-y)] \tag{A-8}$$

$$\cos x \cos y = \frac{1}{2}[\cos(x+y) + \cos(x-y)] \tag{A-9}$$

$$\sin x \sin y = \frac{1}{2}[\cos(x-y) - \cos(x+y)] \tag{A-10}$$

and then to calculate the integrals by using the following definite integrals,

$$\int_0^{2\pi} \cos mx \cos nx \, dx = \begin{cases} 0, & m \neq n \\ \pi, & m = n \neq 0 \end{cases} \tag{A-11}$$

$$\int_0^{2\pi} \sin mx \sin nx \, dx = \begin{cases} 0, & m \neq n \\ \pi, & m = n \neq 0 \end{cases} \tag{A-12}$$

$$\int_0^{2\pi} \cos mx \sin nx \, dx = 0 \tag{A-13}$$

Evaluation of Equations A-3 through A-7 for $r_b(\theta) = r_o$ yields

$$\left(\frac{\partial E_H^1}{\partial r_n}\right)_o = 2\pi M_s H_1 \int_0^{2\pi} \frac{r_o^2}{2} \{\cos[(n+1)\theta - n\theta_n] + \cos[(n-1)\theta - n\theta_n]\} d\theta$$

$$= \begin{cases} 0, & n = 0, \; n \geq 2 \\ 2\pi r_o^2 \pi M_s H_1 \cos\theta_1, & n = 1 \end{cases} \tag{A-14}$$

$$\left(\frac{\partial E_H^1}{\partial \theta_n}\right)_o = 0 \ , \quad \text{for all } n \tag{A-15}$$

$$\left(\frac{\partial^2 E_H^1}{\partial r_n \partial r_m}\right)_o = 4hM_s H_1 \int_0^{2\pi} \frac{r_o}{2} \{\cos[(m+n)\theta - (m\theta_m + n\theta_n)] + \cos[(m-n)\theta - (m\theta_m - n\theta_n)]\}\cos\theta \, d\theta$$

$$= \begin{cases} 0 \ , & m = n \\ 4\pi r_o hM_s H_1 \cos\theta_1 \ , & \begin{matrix} n=0,\ m=1 \\ n=1,\ m=0 \end{matrix} \\ 2\pi r_o hM_s H_1 \cos(n\theta_n - m\theta_m) \ , & |n-m|=1,\ n,m\neq 0 \end{cases} \tag{A-16}$$

$$\left(\frac{\partial^2 E_H^1}{\partial \theta_n \partial \theta_m}\right)_o = 0 \ , \quad \text{for all } n, m \tag{A-17}$$

$$\left(\frac{\partial^2 E_H^1}{\partial r_n \partial \theta_m}\right)_o = 2hM_s H_1 \int_0^{2\pi} \frac{r_o^2}{2} \delta_{mn} n \{\sin[(n+1)\theta - n\theta_n] + \sin[(n-1)\theta - n\theta_n]\} \, d\theta$$

$$= \begin{cases} 0 \ , & n, m \neq 1 \\ -2\pi r_o^2 hM_s H_1 \sin\theta_1 \ , & n = m = 1 \end{cases} \tag{A-18}$$

applying the same procedures to the other two terms, E_H^0 and E_H^1, the resulting nonzero terms were shown in Equations 24 and 26.

VIII. APPENDIX B

The domains observed in orthoferrites are never precisely circular but always have some degree of ellipticity. In the orthoferrites $K_u \gg 2 M_s^2$ so that the magnetization lies rigidly along the plate normal and the wall width is narrow as compared to the domain diameter. The applied field energy, E_H, and the internal magnetostatic energy, E_M, terms of the total energy expression, Equation 4, thus make no contribution to producing the domain anisotropy. Therefore, the anisotropy results from an anisotropy in the wall energy density σ_w. Considering the wall energy density to be independent of wall curvature and the wall to be orientated with its normal perpendicular to the plate normal, the wall energy density is given by (39, 46)

$$\sigma_w = \bar{\sigma}_w + \frac{1}{2} \Delta\sigma_w \cos 2\nu \qquad \text{(B-1)}$$

where $\bar{\sigma}_w$ is the isotropic wall energy density and ν is the angle between the wall normal and the x-axis (see Figure B-1). Equation B-1 implies that the wall energy is maximized when the wall normal lies along the x-axis.

The total wall energy is

$$E_w = h \oint \sigma_w \, ds \qquad \text{(B-2)}$$

where s is arc length along the curve describing the domain shape in the plane. It can be seen from Figure B-1 that ν is related to θ by

$$\theta = \beta + \nu \qquad \text{(B-3)}$$

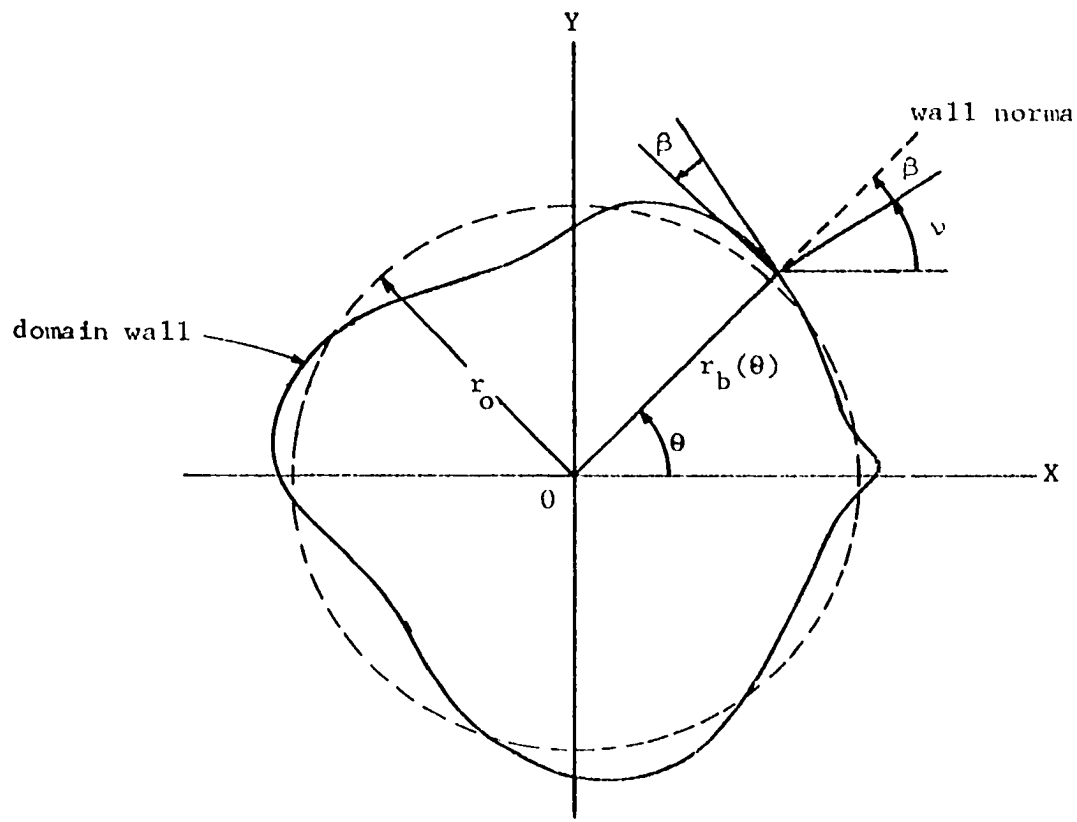

Figure B-1. Coordinate system used in consideration of anisotropy wall energy

Using domain radius function $r_b(\theta)$, Equation 2, $\cos\beta$ can be expressed by

$$\cos\beta = \frac{r_b(\theta)}{\left[r_b^2(\theta)+\left(\frac{\partial r_b(\theta)}{\partial\theta}\right)^2\right]^{\frac{1}{2}}} \tag{B-4}$$

Thus,

$$\cos 2\nu = \cos(2\theta - 2\beta)$$

$$= \cos 2\theta - \frac{2\left(\frac{\partial r_b}{\partial\theta}\right)^2}{r_b^2 + \left(\frac{\partial r_b}{\partial\theta}\right)^2}\cos 2\theta + \frac{2r_b\frac{\partial r_b}{\partial\theta}}{r_b^2 + \left(\frac{\partial r_b}{\partial\theta}\right)^2}\sin 2\theta \tag{B-5}$$

and the differential arc length,

$$ds = \left[r_b^2 + \left(\frac{\partial r_b}{\partial\theta}\right)^2\right]^{\frac{1}{2}} d\theta \tag{B-6}$$

When Equations B-1, B-5, and B-6 are substituted into Equation B-2, the total wall energy expression becomes

$$E_w = h\,\overline{\sigma}_w \int_0^{2\pi}\left[r_b^2 + \left(\frac{\partial r_b}{\partial\theta}\right)^2\right]^{\frac{1}{2}} d\theta$$

$$+ \frac{1}{2} h\,\Delta\sigma_w \int_0^{2\pi}\left\{\left[r_b^2 + \left(\frac{\partial r_b}{\partial\theta}\right)^2\right]^{\frac{1}{2}}\cos 2\theta\right.$$

$$\left. - 2\left(\frac{\partial r_b}{\partial\theta}\right)\left(\frac{\partial r_b}{\partial\theta}\cos 2\theta - r_b\sin 2\theta\right)\left[r_b^2 + \left(\frac{\partial r_b}{\partial\theta}\right)^2\right]^{-\frac{1}{2}}\right\} d\theta \tag{B-7}$$

The first term in Equation B-7 is identical to the isotropic wall energy expression and the second term representing entirely the effect of wall energy anisotropy.

The effect of the anisotropy term can be evaluated by obtaining all the first and second derivatives with respect to Δr_n and $\Delta\theta_n$ of

the expansion of $r_b(\theta)$ for the case of a strictly circular domain, $r_b(\theta)$. The same technique and notations as in Appendix A are used to calculate these partial derivatives. The first derivatives with respect to Δr_n and $\Delta\theta_n$ are

$$\frac{\partial E_w}{\partial r_n} = h\,\overline{\sigma}_w \int_0^{2\pi} \left[r_b \frac{\partial r_b}{\partial r_n} + \frac{\partial r_b}{\partial \theta} \frac{\partial\left(\frac{\partial r_b}{\partial r_n}\right)}{\partial r_n} \right] \left[r_b^2 + \left(\frac{\partial r_b}{\partial \theta}\right)^2 \right]^{-\frac{1}{2}} d\theta$$

$$+ \frac{1}{2} h \Delta\sigma_w \int_0^{2\pi} \left\{ \left[r_b \frac{\partial r_b}{\partial r_n} + \frac{\partial r_b}{\partial \theta} \frac{\partial\left(\frac{\partial r_b}{\partial \theta}\right)}{\partial r_n} \right] \left[r_b^2 + \left(\frac{\partial r_b}{\partial \theta}\right)^2 \right]^{-\frac{1}{2}} \cos 2\theta \right.$$

$$- 2 \frac{\partial\left(\frac{\partial r_b}{\partial \theta}\right)}{\partial r_n} \left(\frac{\partial r_b}{\partial \theta} \cos 2\theta - r_b \sin 2\theta\right) \left[r_b^2 + \left(\frac{\partial r_b}{\partial \theta}\right)^2 \right]^{-\frac{1}{2}}$$

$$\left. - 2 \left(\frac{\partial r_b}{\partial \theta}\right) \frac{\partial}{\partial r_n} \left[\left(\frac{\partial r_b}{\partial \theta} \cos 2\theta - r_b \sin 2\theta\right) \left(r_b^2 + \left(\frac{\partial r_b}{\partial \theta}\right)^2 \right)^{-\frac{1}{2}} \right] \right\} d\theta \tag{B-8}$$

and

$$\frac{\partial E_w}{\partial \theta_n} = h\,\overline{\sigma}_w \int_0^{2\pi} \left[r_b \frac{\partial r_b}{\partial \theta_n} + \frac{\partial r_b}{\partial \theta} \frac{\partial\left(\frac{\partial r_b}{\partial \theta}\right)}{\partial \theta_n} \right] \left[r_b^2 + \left(\frac{\partial r_b}{\partial \theta}\right)^2 \right]^{-\frac{1}{2}} d\theta$$

$$+ \frac{1}{2} h \Delta\sigma_w \int_0^{2\pi} \left\{ \left[r_b \left(\frac{\partial r_b}{\partial \theta_n}\right) + 2 \frac{\partial r_b}{\partial \theta} \frac{\partial\left(\frac{\partial r_b}{\partial \theta}\right)}{\partial \theta_n} \right] \left[r_b^2 + \left(\frac{\partial r_b}{\partial \theta}\right)^2 \right]^{-\frac{1}{2}} \cos 2\theta \right.$$

$$- 2 \frac{\partial\left(\frac{\partial r_b}{\partial \theta}\right)}{\partial \theta_n} \left(\frac{\partial r_b}{\partial \theta} \cos 2\theta - r_b \sin 2\theta\right) \left[r_b^2 + \left(\frac{\partial r_b}{\partial \theta}\right)^2 \right]^{-\frac{1}{2}}$$

$$\left. - 2 \left(\frac{\partial r_b}{\partial \theta}\right) \frac{\partial}{\partial \theta_n} \left[\left(\frac{\partial r_b}{\partial \theta} \cos 2\theta - r_b \sin 2\theta\right) \left(r_b^2 + \left(\frac{\partial r_b}{\partial \theta}\right)^2 \right)^{-\frac{1}{2}} \right] \right\} d\theta \tag{B-9}$$

respectively. Setting $r_b(\theta) = r_o$, $\partial r_b/\partial\theta = 0$, and carrying out the integration by using those definite integrals shown in Appendix A yield

$$\left(\frac{\partial E_w}{\partial r_n}\right)_o = 2\pi h \bar{\sigma}_w \delta_{no} - \frac{3\pi}{2} h \Delta\sigma_w \delta_{n2} \cos 2\theta_2 \tag{B-10}$$

and

$$\left(\frac{\partial E_w}{\partial \theta_n}\right)_o = 0 \tag{B-11}$$

where δ_{mn} is the Kronecker delta function. The remaining derivatives can be computed by the entirely similar manner and the results are

$$\left(\frac{\partial^2 E_w}{\partial r_n \partial r_m}\right)_o = \frac{\pi}{r_o} h \bar{\sigma}_w n^2 \delta_{mn} + \frac{3\pi}{4r_c} h \Delta\sigma_w mn \{\delta_{m1}\delta_{n1} \cos 2\theta_1 - \delta_{n,m\pm 2} \cos(n\theta_n - m\theta_m)\} \tag{B-12}$$

$$\left(\frac{\partial^2 E_w}{\partial r_n \partial \theta_n}\right)_o = 3\pi h \Delta\sigma_w \delta_{m2}\delta_{n2} \sin 2\theta_2 \tag{B-13}$$

and

$$\left(\frac{\partial^2 E_w}{\partial \theta_n \partial \theta_m}\right)_o = 0 \tag{B-14}$$

It can be seen that contributions from $\bar{\sigma}_w$ are the same as in the isotropic case, Equation 6, so that adding the terms of Equations B-10 through B-14 in $\Delta\sigma_w$ to Equation 6 yields the total energy expansion for the anisotropic case. The domain is therefore in equilibrium when the force equation for the isotropic case with $\sigma_w = \bar{\sigma}_w$ is solved and inclusion of the effect of $\Delta\sigma_w$ terms and the second order energy variation solves the elliptical equilibrium problem. It also can be seen that there exists a torque, $-\partial[\Delta r_2 (\partial E_w/\partial r_2)_o]/\partial\theta_2 = -\Delta r_2 (\partial^2 E_w/\partial\theta_2 \partial r_2)_o$, tending to turn an elliptical domain into the direction in which the force tending to make the domain elliptical is most positive.

To solve the equilibrium problem, the gradient of total energy is set to be equal to zero. It yields that the stable equilibrium is obtained when r_o is the stable solution to the isotropic force equation with $\sigma_w = \bar{\sigma}_w$, $\theta_n = 0$, and $\Delta\theta_n = 0$ for all n, and $\Delta r_n = 0$ for $n = 0$ and n odd. The remaining even Δr_n can be determined by using matrix theory. However, the elliptical change in domain shape can be determined easily to the lowest order. The Δr_2 contribution from $\Delta\sigma_w$ is added to the normalized energy variation expression, Equation 8. Setting this equal to zero with r_o being the stable solution to the isotropic force equation yields

$$\frac{3h}{2r_o}\left[\frac{\ell}{h} - S_2\left(\frac{d}{h}\right)\right]\left(\frac{\Delta r_2}{h}\right)^2 - \frac{3}{4}\Delta\ell\,\frac{\Delta r_2}{h^2} = 0 \qquad \text{(B-15)}$$

where

$$\Delta\ell = \frac{\Delta\sigma_w}{4\pi M_s^2} \qquad \text{(B-16)}$$

Thus, the ellipticity due to anisotropic wall energy is given by

$$\frac{\Delta r_2}{r_o} = \frac{1}{2}\,\frac{\Delta\ell}{h\left[\frac{\ell}{h} - S_2\left(\frac{d}{h}\right)\right]} \qquad \text{(B-17)}$$

IX. APPENDIX C

With the coordinate system as shown in Figure 16, the vector magnetic potential from a circular current loop is

$$\vec{A} = \vec{a}_{\phi} \frac{Ir_o}{c} \int_0^{2\pi} \frac{d\phi'}{[r_o^2 + \rho^2 - 2r_o \rho \cos(\phi - \phi') + z^2]^{\frac{1}{2}}} \tag{C-1}$$

where $\vec{a}_{\phi}$ is the unit vector in the ϕ direction. Since there is no ϕ dependence, the integral can be evaluated at a point on the $\phi = 0$ axis. Each contribution to the vector $\vec{A}$ from the individual differential current elements is a vector which is parallel to the current element. This means that as the integration is performed, the components in the x direction will cancel out. Since

$$\vec{a}_{\phi} = -\vec{a}_x \sin\phi + \vec{a}_y \cos\phi \tag{C-2}$$

The vector magnetic potential expression becomes

$$\vec{A} = \vec{a}_y \frac{2Ir_o}{c} \int_0^{2\pi} \frac{\cos\phi' \, d\phi'}{[r_o^2 + \rho^2 - 2r_o \rho \cos\phi' + z^2]^{\frac{1}{2}}} \tag{C-3}$$

Introducing the parameter

$$k^2 = \frac{4r_o \rho}{(r_o + \rho)^2 + z^2} \tag{C-4}$$

and making the change of variable $\phi' = 2\theta$, it is possible to evaluate the vector magnetic potential as:

$$A_{\phi} = \frac{2Ik}{c} \left(\frac{r_o}{\rho}\right)^{\frac{1}{2}} \left[\left(\frac{2}{k^2} - 1\right)K(k) - \frac{2}{k^2} E(k)\right] \tag{C-5}$$

where K and E are the complete elliptic integrals of the first and second kind. It is clear that the vector $\vec{A}$ is only in the ϕ direction. Since

$$\vec{B} = \vec{\nabla} \times \vec{A} \tag{C-6}$$

the radial component of $\vec{B}$ can be calculated by (in cylindrical coordinates)

$$B_\rho = - \frac{\partial A_\phi}{\partial z} \tag{C-7}$$

By using the formulae (47)

$$\frac{\partial K}{\partial k} = \frac{E}{k(1 - k^2)} - \frac{K}{k} \tag{C-8}$$

$$\frac{\partial E}{\partial k} = \frac{E - K}{k} \tag{C-9}$$

Equation C-7 becomes

$$B_\rho = \frac{I z k}{c r_o^{\frac{1}{2}} \rho^{\frac{1}{2}}} \left[\frac{1 - \frac{k^2}{2}}{1 - k^2} E(k) - K(k) \right] \tag{C-10}$$

Consequently, the radial component of magnetic field from a thin cylindrical current sheet of height h can be evaluated by integrating over the entire height. It becomes

$$H_\rho = \frac{I}{c r_o^{\frac{1}{2}} \rho^{\frac{1}{2}}} \int_z^{z\text{th}} \left[\frac{1 - \frac{k^2}{2}}{1 - k^2} E(k) - K(k) \right] k z' dz' \tag{C-11}$$

From Equation C-4,

$$z' dz' = - \frac{4 r_o \rho}{k^3} dk \tag{C-12}$$

thus Equation C-11 becomes

$$H_\rho = -\frac{4I}{c}\left(\frac{r_o}{\rho}\right)^{\frac{1}{2}} \int_{k_1}^{k_2} \left[\frac{1}{k^2}\left(\frac{1-\frac{k^2}{2}}{1-k^2}\right)E(k) - \frac{1}{k^2}K(k)\right]dk \qquad \text{(C-13)}$$

where

$$k_1^2 = \frac{4r_o\rho}{z^2 + (r_o+\rho)^2} \qquad \text{(C-14)}$$

and

$$k_2^2 = \frac{4r_o\rho}{(z+h)^2 + (r_o+\rho)^2} \qquad \text{(C-15)}$$

Rearranging and integrating of Equation C-13 yield

$$H_\rho = -\frac{4I}{c}\left(\frac{r_o}{\rho}\right)^{\frac{1}{2}} \int_{k_1}^{k_2} \left[\frac{E(k) - (1-k^2)K(k)}{k^2(1-k^2)} - \frac{1}{2}\frac{E(k)}{1-k^2}\right]dk$$

$$= -\frac{4I}{c}\left(\frac{r_o}{\rho}\right)^{\frac{1}{2}}\left[\frac{E(k) - K(k)}{k} - \frac{1}{2}k\,K(k)\right]\Bigg|_{k_1}^{k_2}$$

$$= \frac{2I}{c}\left(\frac{r_o}{\rho}\right)^{\frac{1}{2}}\left\{\left[2\,\frac{E(k_1) - K(k_1)}{k_1} - k_1K(k_1)\right]\right.$$

$$\left. - \left[2\,\frac{E(k_2) - K(k_2)}{k_2} - k_2\,K(k_2)\right]\right. \qquad \text{(C-16)}$$

Now the change of source from the current sheet to the magnetization of the bubble may follow the standard method which is

$$2\,M_s = \frac{I}{c} \qquad \text{(C-17)}$$

where the factor of 2 comes from the fact that the bubble is located in a platelet of opposite magnetization. Consequently, the total radial magnetic field from a bubble of thickness h is given by

$$H_\rho = 4 M_s \left(\frac{r_o}{\rho}\right)^{\frac{1}{2}} \left\{\left[2 \frac{E(k_1) - K(k_1)}{k_1} - k_1 K(k_1)\right]\right.$$

$$\left. - \left[2 \frac{E(k_2) - K(k_2)}{k_2} - k_2 K(k_2)\right]\right\} \qquad \text{(C-18)}$$